On the stability of projection-based linear reduced-order models: Descriptor vs non-descriptor forms

D. Amsallem[a,*], C. Farhat[b]

[a]*Department of Aeronautics and Astronautics, Durand Building, 496 Lomita Mall, Stanford University, Stanford, 94305-4035, USA*

[b]*Department of Aeronautics and Astronautics, Department of Mechanical Engineering, and Institute for Computational & Mathematical Engineering, Durand Building, 496 Lomita Mall, Stanford University, Stanford, 94305-4035, USA*

Abstract

Two comprehensive approaches are considered for constructing projection-based reduced-order computational models for linear dynamical systems. The first one reduces the governing equations written in the descriptor form, using a Galerkin or Petrov-Galerkin projection onto a reduced-order basis or pair of them, respectively. These bases can be constructed by any preferred method such as the Proper Orthogonal Decomposition, Balanced Proper Orthogonal Decomposition, or Moment Matching method. The second approach transforms first the governing equations into their non-descriptor form before applying the same projection-based model order reduction method. For several structural and coupled fluid-structure dynamical systems, it is observed that the first reduction approach leads to reduced-order models that exhibit significantly better numerical stability and accuracy properties than those resulting from the second one. These observations are reinforced by theoretical results that anticipate and confirm the better stability properties obtained in general when reducing the descriptor rather than non-descriptor form of the equations governing a linear dynamical system.

Keywords: Balanced POD; Descriptor form; Galerkin projection; LTI dynamical system; Model reduction; Moment matching; Non-descriptor form; Petrov-Galerkin projection; POD; Stability

1. Introduction

Linear Time-Invariant (LTI) systems are routinely used to model the dynamic behavior of electrical, structural, fluid, thermal, and biological systems, to name only a few. Projection-based Model Order Reduction (MOR) methods reduce the dimensionality of LTI systems by projecting them onto carefully chosen Reduced Order Bases (ROBs). For many applications, MOR methods have demonstrated the ability to preserve the accuracy of large-scale LTI systems [1, 2, 3, 4, 5, 6, 7, 8]. However, perserving their numerical stability properties has proved to be a much greater challenge [9, 10]. A few techniques have been successfully proposed for stabilizing LTI Reduced-Order Models (ROMs) [11, 10]. However, these are not without limitations and do not necessarily lead to best-practices in MOR. On the other hand, this paper reports on some observations that point to one simple and frequent source of numerical instability in MOR. It also presents theoretical results that support these observations and lead to at least two best-practice guidelines for performing MOR.

More specifically, this paper considers two different forms of LTI systems. The first one, known as the *descriptor* form, corresponds to the original form of an LTI system in which a matrix $\mathbf{E}$ that is not necessarily the identity pre-multiplies the state time-derivative. The second form, known as the *non-descriptor* form,

*Corresponding author

Email addresses: amsallem@stanford.edu (D. Amsallem), cfarhat@stanford.edu (C. Farhat)

URL: stanford.edu/~amsallem (D. Amsallem)

results from the pre-multiplication of the *descriptor* form of the LTI system by $\mathbf{E}^{-1}$, when $\mathbf{E}$ is invertible. Whereas both descriptor and non-descriptor forms of a given LTI system are mathematically equivalent, their projections onto a given ROB generate two ROMs whose numerical properties are observed in this paper to differ. Furthermore, it is also proved in this paper that Galerkin-based MOR methods applied to the descriptor form of LTI systems deliver ROMs that are less prone to numerical instability than when they are applied to the non-descriptor form of these systems. Therefore, two major contributions of this paper are the advocacy of Galerkin-based projections over Petrov-Galerkin counterparts when both types of projections are feasible for MOR, and their application to the descriptor rather than non-descriptor form of LTI systems.

To this effect, the remainder of this paper is organized as follows. In Section 2, the linear time-invariant equations of interest are introduced. In Section 3, the stability of LTI systems is defined for both descriptor and non-descriptor forms. In Section 4, the reduction of both descriptor and non-descriptor forms of an LTI system is discussed, together with the numerical stability of the resulting ROMs. In Section 5, theoretical results associated with the MOR of structural dynamic and coupled fluid-structure systems are presented and illustrated with numerical computations. Finally, conclusions are offered in Section 6.

2. LTI systems

In this work, first-order LTI systems of the following form are considered

$$\begin{aligned} \mathbf{E}\frac{d\mathbf{x}}{dt}(t) &= \mathbf{A}\mathbf{x}(t) + \mathbf{B}\mathbf{u}(t) \\ \mathbf{y}(t) &= \mathbf{C}\mathbf{x}(t) + \mathbf{D}\mathbf{u}(t), \end{aligned} \tag{1}$$

where t denotes time, $\mathbf{x} \in \mathbb{R}^n$ the vector of state variables, $\mathbf{u} \in \mathbb{R}^p$ the vector of inputs and $\mathbf{y} \in \mathbb{R}^q$ the vector of outputs, and $\mathbf{E} \in \mathbb{R}^{n\times n}$, $\mathbf{A} \in \mathbb{R}^{n\times n}$, $\mathbf{B} \in \mathbb{R}^{n\times p}$, $\mathbf{C} \in \mathbb{R}^{q\times n}$ and $\mathbf{D} \in \mathbb{R}^{q\times p}$ the time-invariant matrices describing the behavior of the physical system of interest. Throughout this paper, $\mathbf{E}$ is assumed to be non-singular. In Computational Fluid Dynamics (CFD), this matrix can be, for example, the diagonal matrix of control volumes arising from the semi-discretization by the finite volume method of the governing Euler or Navier-Stokes equations. In finite element methods for structural dynamics (in state space form) and heat convection, it is typically the mass matrix.

Given an LTI system such as (1), the following complex-valued transfer function can be defined

$$\mathbf{H} : s \in \mathbb{C} \longmapsto \mathbf{C}(s\mathbf{E} - \mathbf{A})^{-1}\mathbf{B} + \mathbf{D} \in \mathbb{C}^{q\times p}. \tag{2}$$

When $\mathbf{E} \neq \mathbf{I}_n$, the LTI system (1) is said to be in *descriptor form*. Since $\mathbf{E}$ is assumed here to be non-singular[1], it can be rewritten as

$$\begin{aligned} \frac{d\mathbf{x}}{dt}(t) &= \mathbf{E}^{-1}\mathbf{A}\mathbf{x}(t) + \mathbf{E}^{-1}\mathbf{B}\mathbf{u}(t) \\ \mathbf{y}(t) &= \mathbf{C}\mathbf{x}(t) + \mathbf{D}\mathbf{u}(t), \end{aligned} \tag{3}$$

which is known as the *non-descriptor form* of the above LTI system. This form is popular, for example, in CFD, as it allows to weight the residual in a given control volume by the inverse of this volume in order to emphasize the regions of the computational domain associated with boundary layers where the mesh resolution is typically finer. The transformation from the descriptor to the non-descriptor form is also often performed to enable the application of a popular MOR method to an LTI system. In this case, a transfer function associated with the system (3) is

$$\mathbf{H} : s \in \mathbb{C} \longmapsto \mathbf{C}(s - \mathbf{E}^{-1}\mathbf{A})^{-1}\mathbf{E}^{-1}\mathbf{B} + \mathbf{D} \in \mathbb{C}^{q\times p}. \tag{4}$$

[1]For the more general case where $\mathbf{E}$ is singular and therefore there is no alternative to the descriptor form of an LTI system, model reduction is studied in [12] and [13]

This transfer function is equal to its counterpart (2).

Throughout the remainder of this paper, both systems (1) and (3) are equipped with the initial condition $\mathbf{x}(0) = \mathbf{x}_0 \in \mathbb{R}^n$.

3. Stability

All High-Dimensional computational Models (HDM) of the form (1) or (3) considered in this paper are assumed to be stable in the following sense.

Definition 1. The system (1) (respectively (3)) is said to be *asympotically stable* if $\lim_{t\to\infty} \mathbf{x}(t) = \mathbf{0}$, for every solution $\mathbf{x}(t)$ of $\mathbf{E}\dfrac{d\mathbf{x}}{dt}(t) = \mathbf{A}\mathbf{x}(t)$ $\big($respectively $\dfrac{d\mathbf{x}}{dt}(t) = \mathbf{E}^{-1}\mathbf{A}\mathbf{x}(t)\big)$.

Remark 1. Since systems (1) and (3) are equivalent, asymptotic stability for one form is equivalent to asymptotic stability for the other.

Next, a Lyapunov function is defined as follows.

Definition 2. $\mathcal{V} : \mathbb{R}^n \to [0, \infty)$ is a Lyapunov function for system (1) $\big($respectively (3)$\big)$ if:

1. $\mathcal{V}(\mathbf{x}) = 0$ if and only if $\mathbf{x} = \mathbf{0}$.
2. For every solution $\mathbf{x}(t)$ of $\mathbf{E}\dfrac{d\mathbf{x}}{dt}(t) = \mathbf{A}\mathbf{x}(t)$ $\big($respectively $\dfrac{d\mathbf{x}}{dt}(t) = \mathbf{E}^{-1}\mathbf{A}\mathbf{x}(t)\big)$, the following inequality holds
$$\frac{d}{dt}\mathcal{V}(\mathbf{x}(t)) \leq 0. \tag{5}$$

Then, the following theorem holds [14].

Theorem 1. If the system (1) $\big($respectively (3)$\big)$ has a Lyapunov function $\mathcal{V}$, it is asymptotically stable.

Example 1. If $\mathcal{V}(\mathbf{x}) = \mathbf{x}^T \left(\mathbf{E}^T\mathbf{P}\mathbf{E}\right)\mathbf{x}$, where $\mathbf{P}$ is a symmetric positive definite matrix, the inequality (5) can also be written in the case of the descriptor form as

$$\mathbf{E}^T\mathbf{P}\mathbf{A} + \mathbf{A}^T\mathbf{P}\mathbf{E} = -\mathbf{Q}_{\mathrm{D}}, \tag{6}$$

where $\mathbf{Q}_{\mathrm{D}}$ is a symmetric positive definite matrix.

Similarly, if $\mathcal{V}(\mathbf{x}) = \mathbf{x}^T\mathbf{P}\mathbf{x}$, where $\mathbf{P}$ is a symmetric positive definite matrix, the inequality (5) can also be written in the case of the non-descriptor form as

$$\mathbf{P}\mathbf{E}^{-1}\mathbf{A} + \mathbf{A}^T\mathbf{E}^{-T}\mathbf{P} = -\mathbf{Q}_{\mathrm{ND}}, \tag{7}$$

where $\mathbf{Q}_{\mathrm{ND}}$ is also a symmetric positive definite matrix.

4. Projection-based model order reduction

Whether applied to the descriptor (1) or non-descriptor (3) form of an LTI system, a projection-based MOR method generates another LTI system of much smaller dimension $k << n$. In general, such an MOR method operates with two ROBs:

- A trial ROB $\mathbf{V}_k \in \mathbb{R}^{n\times k}$ with full-column rank, introduced to approximate the state vector $\mathbf{x}(t)$ as
$$\mathbf{x}(t) \approx \mathbf{V}_k\mathbf{x}_k(t). \tag{8}$$
The approximate state vector is then uniquely defined by the vector of generalized coordinates $\mathbf{x}_k \in \mathbb{R}^k$. Substituting the above approximation into the original LTI system yields a non-zero residual $\mathbf{r}(t) \in \mathbb{R}^n$.
- A test ROB $\mathbf{W}_k$ with full-column rank as well, introduced to limit the size of the residual $\mathbf{r}(t)$ by constraining it to satisfy the orthogonality condition $\mathbf{W}_k^T\mathbf{r}(t) = \mathbf{0}$.

When $\mathbf{W}_k \neq \mathbf{V}_k$, the projection-based MOR method is a Petrov-Galerkin approximation method. When $\mathbf{W}_k = \mathbf{V}_k$, it becomes a Galerkin approximation method.

The next two sections focus on the form of a projected LTI system originally written in descriptor or non-descriptor form. Then, the impact of the form of the expression of the LTI system and the type of the projection method on the numerical stability of the constructed ROM is discussed in the context of popular methods for constructing ROBs.

4.1. Reduction of an LTI system written in descriptor form

Once a trial ROB $\mathbf{V}_k$ has been constructed, the state vector is approximated as in (8). Substituting this approximation into the original system (1) gives

$$\begin{aligned} \mathbf{E}\mathbf{V}_k \frac{d\mathbf{x}_k}{dt}(t) &= \mathbf{A}\mathbf{V}_k\mathbf{x}_k(t) + \mathbf{B}\mathbf{u}(t) + \mathbf{r}(t) \\ \mathbf{y}(t) &= \mathbf{C}\mathbf{V}_k\mathbf{x}_k(t) + \mathbf{D}\mathbf{u}(t). \end{aligned} \tag{9}$$

Next, forcing the residual $\mathbf{r}(t)$ to be orthogonal to the test ROB $\mathbf{W}_k$ leads to the following ROM of the LTI system

$$\begin{aligned} \left(\mathbf{W}_k^T\mathbf{E}\mathbf{V}_k\right) \frac{d\mathbf{x}_k}{dt}(t) &= \left(\mathbf{W}_k^T\mathbf{A}\mathbf{V}_k\right)\mathbf{x}_k(t) + \mathbf{W}_k^T\mathbf{B}\mathbf{u}(t) \\ \mathbf{y}(t) &= \mathbf{C}\mathbf{V}_k\mathbf{x}_k(t) + \mathbf{D}\mathbf{u}(t). \end{aligned} \tag{10}$$

The counterpart of the above ROM generated by a Galerkin projection is obtained by setting $\mathbf{W}_k = \mathbf{V}_k$, which gives

$$\begin{aligned} \left(\mathbf{V}_k^T\mathbf{E}\mathbf{V}_k\right) \frac{d\mathbf{x}_k}{dt}(t) &= \left(\mathbf{V}_k^T\mathbf{A}\mathbf{V}_k\right)\mathbf{x}_k(t) + \mathbf{V}_k^T\mathbf{B}\mathbf{u}(t) \\ \mathbf{y}(t) &= \mathbf{C}\mathbf{V}_k\mathbf{x}_k(t) + \mathbf{D}\mathbf{u}(t). \end{aligned} \tag{11}$$

In general, the trial and test ROBs are chosen to be bi-orthogonal with respect to a well-chosen operator. When operating on a descriptor form, $\mathbf{V}_k$ and $\mathbf{W}_k$ are often chosen so that $\mathbf{W}_k^T\mathbf{E}\mathbf{V}_k = \mathbf{I}_k$. In this case, the ROM of the LTI system can be written as

$$\begin{aligned} \frac{d\mathbf{x}_k}{dt}(t) &= \mathbf{A}_k\mathbf{x}_k(t) + \mathbf{B}_k\mathbf{u}(t) \\ \mathbf{y}(t) &= \mathbf{C}_k\mathbf{x}_k(t) + \mathbf{D}_k\mathbf{u}(t), \end{aligned} \tag{12}$$

where

$$\begin{aligned} \mathbf{A}_k &= \mathbf{W}_k^T\mathbf{A}\mathbf{V}_k \in \mathbb{R}^{k\times k} \\ \mathbf{B}_k &= \mathbf{W}_k^T\mathbf{B} \in \mathbb{R}^{k\times p} \\ \mathbf{C}_k &= \mathbf{C}\mathbf{V}_k \in \mathbb{R}^{q\times k} \\ \mathbf{D}_k &= \mathbf{D} \in \mathbb{R}^{q\times p}. \end{aligned} \tag{13}$$

Denoting the approximated high-dimensional state by $\widehat{\mathbf{x}}(t) = \mathbf{V}_k\mathbf{x}_k(t)$, the following equivalent of the original high-dimensional system can be reconstructed

$$\begin{aligned} \frac{d\widehat{\mathbf{x}}}{dt}(t) &= \left(\mathbf{V}_k\mathbf{W}_k^T\mathbf{A}\right)\widehat{\mathbf{x}}(t) + \left(\mathbf{V}_k\mathbf{W}_k^T\mathbf{B}\right)\mathbf{u}(t) \\ \mathbf{y}(t) &= \mathbf{C}\widehat{\mathbf{x}}(t) + \mathbf{D}\mathbf{u}(t). \end{aligned} \tag{14}$$

This system will be particularly useful when studying the stability of the ROM.

4.2. Reduction of an LTI system written in non-descriptor form

For the LTI system expressed in non-descriptor form, the state approximation (8) results in

$$\begin{aligned} \mathbf{V}_k \frac{d\mathbf{x}_k}{dt}(t) &= \left(\mathbf{E}^{-1}\mathbf{A}\mathbf{V}_k\right)\mathbf{x}_k(t) + \mathbf{E}^{-1}\mathbf{B}\mathbf{u}(t) + \mathbf{r}(t) \\ \mathbf{y}(t) &= \mathbf{C}\mathbf{V}_k\mathbf{x}_k(t) + \mathbf{D}\mathbf{u}(t). \end{aligned} \tag{15}$$

Enforcing the orthogonality of the residual vector $\mathbf{r}(t)$ and the test ROB $\mathbf{W}_k$ yields

$$\begin{aligned} \mathbf{W}_k^T\mathbf{V}_k \frac{d\mathbf{x}_k}{dt}(t) &= \left(\mathbf{W}_k^T\mathbf{E}^{-1}\mathbf{A}\mathbf{V}_k\right)\mathbf{x}_k(t) + \left(\mathbf{W}_k^T\mathbf{E}^{-1}\mathbf{B}\right)\mathbf{u}(t) \\ \mathbf{y}(t) &= \mathbf{C}\mathbf{V}_k\mathbf{x}_k(t) + \mathbf{D}\mathbf{u}(t). \end{aligned} \tag{16}$$

Here, it is noted that whereas equations (15) are equivalent to their descriptor form counterparts (9), the reduced LTI system (16) is not equivalent to its descriptor form counterpart (10). In the case of a Galerkin projection, this system becomes

$$\begin{aligned} \mathbf{V}_k^T\mathbf{V}_k \frac{d\mathbf{x}_k}{dt}(t) &= \left(\mathbf{V}_k^T\mathbf{E}^{-1}\mathbf{A}\mathbf{V}_k\right)\mathbf{x}_k(t) + \left(\mathbf{V}_k^T\mathbf{E}^{-1}\mathbf{B}\right)\mathbf{u}(t) \\ \mathbf{y}(t) &= \mathbf{C}\mathbf{V}_k\mathbf{x}_k(t) + \mathbf{D}\mathbf{u}(t). \end{aligned} \tag{17}$$

If the trial and test ROBs are chosen to be bi-orthogonal with respect to the identity matrix — that is $\mathbf{W}_k^T\mathbf{V}_k = \mathbf{I}_k$, the resulting ROM becomes

$$\begin{aligned} \frac{d\mathbf{x}_k}{dt}(t) &= \mathbf{A}_k\mathbf{x}_k(t) + \mathbf{B}_k\mathbf{u}(t) \\ \mathbf{y}(t) &= \mathbf{C}_k\mathbf{x}_k(t) + \mathbf{D}_k\mathbf{u}(t), \end{aligned} \tag{18}$$

where

$$\begin{aligned} \mathbf{A}_k &= \mathbf{W}_k^T\mathbf{E}^{-1}\mathbf{A}\mathbf{V}_k \in \mathbb{R}^{k\times k} \\ \mathbf{B}_k &= \mathbf{W}_k^T\mathbf{E}^{-1}\mathbf{B} \in \mathbb{R}^{k\times p} \\ \mathbf{C}_k &= \mathbf{C}\mathbf{V}_k \in \mathbb{R}^{q\times k} \\ \mathbf{D}_k &= \mathbf{D} \in \mathbb{R}^{q\times p}. \end{aligned} \tag{19}$$

As in the descriptor case, the following equivalent of the original high-dimensional system written in non-descriptor form can be reconstructed

$$\begin{aligned} \frac{d\widehat{\mathbf{x}}}{dt}(t) &= \left(\mathbf{V}_k\mathbf{W}_k^T\mathbf{E}^{-1}\mathbf{A}\right)\widehat{\mathbf{x}}(t) + \left(\mathbf{V}_k\mathbf{W}_k^T\mathbf{E}^{-1}\mathbf{B}\right)\mathbf{u}(t) \\ \mathbf{y}(t) &= \mathbf{C}\widehat{\mathbf{x}}(t) + \mathbf{D}\mathbf{u}(t). \end{aligned} \tag{20}$$

4.3. Stability of the ROM

In general, a projection-based MOR method with arbitrary ROBs $\mathbf{V}_k$ and $\mathbf{W}_k$ does not preserve the stability of the LTI system to which it is applied. To illustrate this fact, consider the two LTI systems given below

$$\begin{bmatrix} 1 & 0 \\ 0 & 0.5 \end{bmatrix} \frac{d\mathbf{x}}{dt}(t) = \begin{bmatrix} 1 & -3.5 \\ 0.6 & -2 \end{bmatrix} \mathbf{x}(t), \quad \text{and} \quad \frac{d\mathbf{x}}{dt}(t) = \begin{bmatrix} 1 & -3.5 \\ 0.6 & -2 \end{bmatrix} \mathbf{x}(t). \tag{21}$$

The first one is written in descriptor form, and the second one in non-descriptor form. Both systems are asymptotically stable, but the ROM $\dfrac{d\mathbf{x}_1}{dt} = \mathbf{x}_1$ resulting from the Galerkin projection of either of them using the ROBs $\mathbf{V}_1 = \mathbf{W}_1 = \begin{bmatrix} 1 \\ 0 \end{bmatrix}$ is not stable.

However, the following theoretical results show that when the HDM operators satisfy certain properties, stability can be preserved after projection.

Theorem 2. If the operator $\mathbf{A}+\mathbf{A}^T$ is stable — that is, all of its eigenvalues have non-positive real parts — any ROM of the form (12) resulting from the Galerkin projection of an LTI system written in descriptor form is asymptotically stable.

Proof. Let $\mathcal{V}(\mathbf{x}) = \mathbf{x}^T\mathbf{E}\mathbf{x}$, and let $\widehat{\mathbf{x}}$ denote the solution of the ROM problem (14) originating from the descriptor form of the LTI system of interest with $\mathbf{u}(t) = 0$ and $\mathbf{W}_k = \mathbf{V}_k$. Then,

$$\begin{aligned}\frac{d\mathcal{V}(\widehat{\mathbf{x}})}{dt} &= \frac{d\widehat{\mathbf{x}}}{dt}^T \mathbf{E}\widehat{\mathbf{x}} + \widehat{\mathbf{x}}^T\mathbf{E}\frac{d\widehat{\mathbf{x}}}{dt} \\ &= \widehat{\mathbf{x}}^T\left(\mathbf{A}^T\mathbf{V}_k\mathbf{V}_k^T\mathbf{E}\right)\widehat{\mathbf{x}} + \widehat{\mathbf{x}}^T\left(\mathbf{E}\mathbf{V}_k\mathbf{V}_k^T\mathbf{A}\right)\widehat{\mathbf{x}} \\ &= \widehat{\mathbf{x}}^T\left(\mathbf{A}^T\mathbf{V}_k\mathbf{V}_k^T\mathbf{E}\mathbf{V}_k\right)\mathbf{x}_k + \mathbf{x}_k^T\left(\mathbf{V}_k^T\mathbf{E}\mathbf{V}_k\mathbf{V}_k^T\mathbf{A}\right)\widehat{\mathbf{x}}. \end{aligned} \tag{22}$$

If $\mathbf{V}_k^T\mathbf{E}\mathbf{V}_k = \mathbf{I}_k$ and $\mathbf{A}^T + \mathbf{A}$ is stable, then

$$\frac{d\mathcal{V}(\widehat{\mathbf{x}})}{dt} = \left(\widehat{\mathbf{x}}^T\mathbf{A}^T\mathbf{V}_k\right)\mathbf{x}_k + \left(\mathbf{x}_k^T\mathbf{V}_k^T\mathbf{A}\right)\widehat{\mathbf{x}} = \left(\mathbf{V}_k\mathbf{x}_k\right)^T\left(\mathbf{A}^T + \mathbf{A}\right)\left(\mathbf{V}_k\mathbf{x}_k\right) \leq 0. \tag{23}$$

Hence, $\mathcal{V}$ is a Lyapunov function for $\dfrac{d\widehat{\mathbf{x}}}{dt} = \left(\mathbf{V}_k\mathbf{V}_k^T\mathbf{A}\right)\widehat{\mathbf{x}}$ which, using Theorem 1, concludes the proof.

Remark 1. For this choice of function $\mathcal{V}$, there is no analog of the above theorem for the case of a Petrov-Galerkin projection of an LTI system written in descriptor form, as the sign of

$$\frac{d\mathcal{V}(\widehat{\mathbf{x}})}{dt} = \mathbf{x}_k^T\mathbf{V}_k^T(\mathbf{A}^T\mathbf{W}_k\mathbf{V}_k^T\mathbf{E} + \mathbf{E}\mathbf{V}_k\mathbf{W}_k^T\mathbf{A})\mathbf{V}_k\mathbf{x}_k \tag{24}$$

depends on the choice of the ROBs $\mathbf{V}_k$ and $\mathbf{W}_k$. Moreover, a counterexample will be presented in Section 5.1.2 to show that a Petrov-Galerkin projection of an HDM written in descriptor form and satisfying the properties formulated in Theorem 2 does not preserve stability.

For an LTI system expressed in the non-descriptor form, the following analog to Theorem 2 can be established however.

Theorem 3. If the operator $\mathbf{E}^{-1}\mathbf{A} + \mathbf{A}^T\mathbf{E}^{-T}$ is stable, then any ROM of the form (18) resulting from the Galerkin projection of an LTI system written in non-descriptor form is asymptotically stable.

Proof. The proof is identical to that given for the descriptor case using $\mathcal{V}(\mathbf{x}) = \mathbf{x}^T\mathbf{x}$.

Theorem 2 and Theorem 3 highlight an advantage of the Galerkin projection method over its Petrov-Galerkin alternative.

4.4. Sample methods for constructing a ROB

4.4.1. Proper orthogonal decomposition methods

The proper orthogonal decomposition method. The Proper Orthogonal Decomposition (POD) method based on snapshots [15] computes a trial ROB $\mathbf{V}_k$ by compressing the information contained in solution snapshots of the system of interest. For the case of LTI systems, these snapshots can be computed either in the time or in the frequency domain. To simplify the notation, only the case of a single input ($p = 1$) and a single output ($q = 1$) is considered here. This case is easily generalizable to multiple inputs and outputs.

In the time domain, the snapshots are typically obtained by computing the dynamic response of an LTI system for a given forcing input and collecting samples $\{\mathbf{x}(t_i)\}_{i=1}^{N_{\text{snaps}}}$ into a (snapshot) matrix

$$\mathbf{X} = \mathbf{X}(t_1, \cdots, t_{N_{\text{snaps}}}) = \begin{bmatrix}\mathbf{x}(t_1) & \cdots & \mathbf{x}(t_{N_{\text{snaps}}})\end{bmatrix}, \tag{25}$$

where N_{snaps} denotes the number of snapshots.

In the frequency domain, each complex-valued snapshot [3] is computed as the solution of a frequency response problem of the form

$$(j\omega_i\mathbf{E} - \mathbf{A})\mathbf{x}(\omega_i) = \mathbf{B}, \tag{26}$$

where ω_i denotes the sampling circular frequency of interest. Next, these snapshots are stored in a real-valued matrix as follows

$$\mathbf{X} = \mathbf{X}(\omega_1, \cdots, \omega_{N_{\text{snaps}}}) = \left[\text{Re}\left(\mathbf{x}(\omega_1)\right) \quad \ldots \quad \text{Re}\left(\mathbf{x}(\omega_{N_{\text{snaps}}})\right) \quad \text{Im}\left(\mathbf{x}(\omega_1)\right) \quad \ldots \quad \text{Im}\left(\mathbf{x}(\omega_{N_{\text{snaps}}})\right)\right]. \tag{27}$$

Whether collected in the time or frequency domain, the snapshots are independent of the form in which the LTI system is written because both descriptor and non-descriptor forms of such a system are mathematically equivalent. However, as it will be shown below, the trial ROBs $\mathbf{V}_k$ constructed using these snapshots differ.

In the case of an LTI system written in the descriptor form, when $\mathbf{E}$ is symmetric positive definite, the POD method proceeds with computing the eigenvalue decomposition

$$\mathbf{X}^T\mathbf{E}\mathbf{X} = \mathbf{\Phi}^d\mathbf{\Lambda}^d{\mathbf{\Phi}^d}^T, \tag{28}$$

where $\mathbf{X}^T\mathbf{E}\mathbf{X}$ is a small-size matrix. Next, the above decomposition is truncated to the matrices of first k eigenvalues $\mathbf{\Lambda}_k^d$ and corresponding eigenvectors $\mathbf{\Phi}_k^d$, and $\mathbf{V}_k^d$ is constructed as follows

$$\mathbf{V}_k^d = \mathbf{X}\mathbf{\Phi}_k^d{\mathbf{\Lambda}_k^d}^{-\frac{1}{2}} \tag{29}$$

Alternatively, $\mathbf{V}_k^d$ can be constructed by first computing the Singular Value Decomposition (SVD) of the matrix $\mathbf{E}^{\frac{1}{2}}\mathbf{X}$, retaining the first k left singular vectors $\mathbf{Y}_k$, and defining $\mathbf{V}_k^d = \mathbf{E}^{-\frac{1}{2}}\mathbf{Y}_k$. Then, a ROM of the form (12) can be built using a Galerkin projection based on $\mathbf{V}_k^d$.

For an LTI system written in non-descriptor form, the following eigenvalue decomposition is performed instead

$$\mathbf{X}^T\mathbf{X} = \mathbf{\Phi}^{nd}\mathbf{\Lambda}^{nd}{\mathbf{\Phi}^{nd}}^T \tag{30}$$

and $\mathbf{V}_k^{nd}$ is constructed as in (29)[2]. A ROM of the form given in (18) is then constructed using a Galerkin projection based on $\mathbf{V}_k^{nd}$.

In summary, because $\mathbf{\Phi}_k^d \neq \mathbf{\Phi}_k^{nd}$, $\mathbf{V}_k^d \neq \mathbf{V}_k^{nd}$ and the two ROMs constructed by applying of the POD method to both descriptor and non-descriptor forms of the same LTI system using the same snapshots are also different.

The balanced POD method. Information about the outputs of interest can be included in the construction of a ROM. For example, the Balanced Truncation (BT) [1] method constructs trial and test ROBs such that the ROM resulting from the Petrov-Galerkin projection is balanced in the sense that the most observable and controllable states are retained. This method also preserves the stability of the underlying HDM. Unfortunately for very large-scale systems, the computational cost associated with the BT method can be prohibitive. For this reason, the Balanced Proper Orthogonal Decomposition (BPOD) method [4, 16] was developed. This alternative method constructs at a reasonable CPU cost trial and test ROBs that lead to an approximately balanced ROM system, but does not necessarily preserve stability (for example, see Section 5.1.2). More specifically, BPOD relies on two sets of snapshots. The first one is known as the set of primal snapshots. These are identical to the snapshots collected for the POD method. The second set of snapshots is known as the set of dual snapshots. These are constructed using a dual LTI system as summarized below.

For an LTI system written in descriptor form, the dual system is

$$\begin{aligned} \mathbf{E}^T\frac{d\mathbf{z}}{dt}(t) &= -\mathbf{A}^T\mathbf{z}(t) - \mathbf{C}^T\mathbf{v}(t) \\ \mathbf{w}(t) &= \mathbf{B}^T\mathbf{z}(t) + \mathbf{D}^T\mathbf{v}(t), \end{aligned} \tag{31}$$

[2]The trial ROB $\mathbf{V}_k^{nd}$ can be equivalently obtained using the SVD of $\mathbf{X}$

where $\mathbf{z} \in \mathbb{R}^n$ is the dual state vector, $\mathbf{v} \in \mathbb{R}^q$ the vector of inputs, and $\mathbf{w} \in \mathbb{R}^p$ the vector of outputs. Assume that the snapshots are collected in the frequency domain. In this case, each complex-valued dual snapshot $\mathbf{z}^d(\omega_i)$ associated with (31) is defined as the solution of the following frequency response problem

$$(-j\omega_i \mathbf{E}^T - \mathbf{A}^T)\mathbf{z}^d(\omega_i) = \mathbf{C}^T. \tag{32}$$

As described above for the primal snapshots, the dual snapshots are also stored in a real-valued matrix as follows

$$\mathbf{Z}^d = \mathbf{Z}^d(\omega_1, \cdots, \omega_{N_{\text{snaps}}}) = \left[\text{Re}\left(\mathbf{z}^d(\omega_1)\right) \quad \ldots \quad \text{Re}\left(\mathbf{z}^d(\omega_{N_{\text{snaps}}})\right) \quad \text{Im}\left(\mathbf{z}^d(\omega_1)\right) \quad \ldots \quad \text{Im}\left(\mathbf{z}^d(\omega_{N_{\text{snaps}}})\right)\right]. \tag{33}$$

Next, the SVD of the small-size matrix $\mathbf{Z}^{d^T}\mathbf{E}\mathbf{X}$ is performed

$$\mathbf{Z}^{d^T}\mathbf{E}\mathbf{X} = \mathbf{\Psi}^d\mathbf{\Sigma}^d\mathbf{\Phi}^{d^T}, \tag{34}$$

and the first k singular values $\mathbf{\Sigma}_k^d$ and associated left and right singular vectors $\mathbf{\Psi}_k^d$ and $\mathbf{\Phi}_k^d$ are used to construct

$$\mathbf{W}_k^d = \mathbf{Z}^d\mathbf{\Psi}_k^d\mathbf{\Sigma}_k^{d^{-\frac{1}{2}}}, \quad \text{and} \quad \mathbf{V}_k^d = \mathbf{X}^d\mathbf{\Phi}_k^d\mathbf{\Sigma}_k^{d^{-\frac{1}{2}}}. \tag{35}$$

Then, a ROM of the form (10) is obtained using a Petrov-Galerkin projection based on the ROBs $\mathbf{W}_k^d$ and $\mathbf{V}_k$.

Similarly, the dual system of an LTI system expressed in non-descriptor form is given by

$$\begin{aligned} \frac{d\mathbf{z}}{dt}(t) &= -\mathbf{A}^T\mathbf{E}^{-T}\mathbf{z}(t) - \mathbf{C}^T\mathbf{v}(t) \\ \mathbf{w}(t) &= \mathbf{B}^T\mathbf{E}^{-T}\mathbf{z}(t) + \mathbf{D}^T\mathbf{v}(t), \end{aligned} \tag{36}$$

and the complex-valued dual snapshots $\mathbf{z}^{nd}(\omega_i)$ are defined as the solutions of the problems

$$(-j\omega_i\mathbf{I}_n - \mathbf{A}^T\mathbf{E}^{-T})\mathbf{z}^{nd}(\omega_i) = \mathbf{C}^T \tag{37}$$

for multiple circular frequencies ω_i. Note that the comparison of Eq. (37) and Eq. (32) reveals that the dual snapshots associated with both forms of a given LTI system are not identical, but related as follows

$$\mathbf{z}^{nd}(\omega_i) = \mathbf{E}^T\mathbf{z}^d(-\omega_i), \ i = 1, \cdots, N_{\text{snaps}}. \tag{38}$$

The dual snapshots are stored in the matrix

$$\mathbf{Z}^{nd} = \mathbf{Z}^{nd}(\omega_1, \cdots, \omega_{N_{\text{snaps}}}) = \left[\text{Re}\left(\mathbf{z}^{nd}(\omega_1)\right) \quad \ldots \quad \text{Re}\left(\mathbf{z}^{nd}(\omega_{N_{\text{snaps}}})\right) \quad \text{Im}\left(\mathbf{z}^{nd}(\omega_1)\right) \quad \ldots \quad \text{Im}\left(\mathbf{z}^{nd}(\omega_{N_{\text{snaps}}})\right)\right], \tag{39}$$

and the following SVD is performed

$$\mathbf{Z}^{nd^T}\mathbf{X} = \mathbf{\Psi}^{nd}\mathbf{\Sigma}^{nd}\mathbf{\Phi}^{nd^T}. \tag{40}$$

Truncating the first k singular values $\mathbf{\Sigma}_k^{nd}$ and associated left and right singular vectors leads to the definition of the matrices $\mathbf{\Psi}_k^{nd}$ and $\mathbf{\Phi}_k^{nd}$ and to the construction of the test and trial ROBs as follows

$$\mathbf{W}_k^{nd} = \mathbf{Z}^{nd}\mathbf{\Psi}_k^{nd}\mathbf{\Sigma}_k^{nd^{-\frac{1}{2}}}, \quad \mathbf{V}_k^{nd} = \mathbf{X}\mathbf{\Phi}_k^{nd}\mathbf{\Sigma}_k^{nd^{-\frac{1}{2}}}. \tag{41}$$

Again, the Petrov-Galerkin projection based on the above test and trial ROBs leads to a ROM of the form (16).

Focusing for simplicity on the case where the snapshots are computed in the frequency domain, the following theorem shows that, unlike the POD method, the BPOD method constructs the same ROM whether applied to the descriptor or non-descriptor form of the LTI system of interest.

Theorem 4. The ROMs obtained by the application of a Petrov-Galerkin projection based on trial and test bases computed by the BPOD method to the descriptor and non-descriptor forms of an LTI system of interest are identical if the snapshot frequency sampling $\{\omega_i\}_{i=1}^{N_{\text{snaps}}}$ is the same in both cases.

Proof. See the Appendix.

4.4.2. Moment matching methods

The j-th moment of a transfer function $\mathbf{H}(s)$ at $s = s_0$ is defined as

$$\eta_j(s_0) = (-1)^j \frac{d\mathbf{H}^{(j)}}{ds}(s_0),\ j = 0,\ 1,\ 2,\ \cdots \tag{42}$$

For the LTI systems considered in this paper, this moment can be expressed explicitly as

$$\begin{aligned} \eta_0(s_0) &= \mathbf{C}(s_0\mathbf{E} - \mathbf{A})^{-1}\mathbf{B} + \mathbf{D} \\ \eta_j(s_0) &= j!\mathbf{C}(s_0\mathbf{E} - \mathbf{A})^{-(j+1)}\mathbf{B},\ j \geq 1. \end{aligned} \tag{43}$$

It can be shown (for example, see [2, 14]) that the first k moments of an LTI system can be matched by a projection-based MOR method provided that the trial basis $\mathbf{V}_k$ satisfies

$$\text{range}(\mathbf{V}_k) = \text{span}\left\{(s_0\mathbf{E} - \mathbf{A})^{-1}\mathbf{B}, \cdots, (s_0\mathbf{E} - \mathbf{A})^{-k}\mathbf{B}\right\}. \tag{44}$$

Since the transfer function (2) associated with the descriptor form of an LTI system is equal to its counterpart (4) associated with the non-descriptor form of that system, the ranges of the trial bases associated with both forms of the LTI system are identical. The right member of (44) describes a Krylov subspace defined by the vector $(s_0\mathbf{E}-\mathbf{A})^{-1}\mathbf{B}$ and the matrix $(s_0\mathbf{E}-\mathbf{A})^{-1}$. Algorithms for constructing this subspace can be found in [14, 17, 18], for example. In particular, the Arnoldi method constructs a trial ROB that is orthogonal with respect to the identity. For an LTI system written in the descriptor form, a trial ROB satisfying $\mathbf{V}_k^T\mathbf{E}\mathbf{V}_k = \mathbf{I}_k$ can next be constructed by a post-processing step. Then, a ROM can be built using a Galerkin projection based on $\mathbf{V}_k$.

5. Numerical stability: Case studies

5.1. Structural dynamics

5.1.1. LTI systems of interest

Linearized structural dynamics problems are typically modeled by second-order LTI systems of the form

$$\begin{aligned} \mathbf{M}\frac{d^2\mathbf{z}}{dt^2}(t) + \mathbf{D}\frac{d\mathbf{z}}{dt}(t) + \mathbf{K}\mathbf{z}(t) &= \mathbf{F}\mathbf{u}(t) \\ \mathbf{y}(t) &= \mathbf{G}\mathbf{z}(t) + \mathbf{C}\frac{d\mathbf{z}}{dt}(t) + \mathbf{H}\mathbf{u}(t), \end{aligned} \tag{45}$$

where $\mathbf{z} \in \mathbb{R}^n$ denotes the vector of structural displacements, $\mathbf{u}$ and $\mathbf{y}$ the vectors of input and output variables, respectively, $\mathbf{M}$, $\mathbf{D}$ and $\mathbf{K}$ are the mass, damping, and stiffness matrices, respectively, and $\mathbf{F}$, $\mathbf{C}$, $\mathbf{G}$ and $\mathbf{H}$ are time-invariant matrices describing inputs and outputs. The matrices $\mathbf{M}$, $\mathbf{D}$ and $\mathbf{K}$ are typically Symmetric Positive Definite (SPD). Hence, throughout the remainder of this paper, they are assumed to have this property.

Eq. (45) above can be recast in first-order form by introducing the state-vector

$$\mathbf{x} = \begin{bmatrix} \frac{d\mathbf{z}}{dt} \\ \mathbf{z} \end{bmatrix} \tag{46}$$

containing both the displacement and velocity degrees of freedom (dof). This leads to the following first-order LTI system written in descriptor form

$$\begin{aligned} \begin{bmatrix} \mathbf{M} & \mathbf{0} \\ \mathbf{0} & \mathbf{J} \end{bmatrix} \frac{d\mathbf{x}}{dt}(t) &= \begin{bmatrix} -\mathbf{D} & -\mathbf{K} \\ \mathbf{J} & \mathbf{0} \end{bmatrix} \mathbf{x}(t) + \begin{bmatrix} \mathbf{F} \\ \mathbf{0} \end{bmatrix} \mathbf{u}(t) \\ \mathbf{y}(t) &= \begin{bmatrix} \mathbf{C} & \mathbf{G} \end{bmatrix} \mathbf{x}(t) + \mathbf{H}\mathbf{u}(t), \end{aligned} \tag{47}$$

where $\mathbf{J} \in \mathbb{R}^{n\times n}$ is an arbitrary non-singular matrix. The above system can also be written in non-descriptor form as follows

$$\begin{aligned} \frac{d\mathbf{x}}{dt}(t) &= \begin{bmatrix} -\mathbf{M}^{-1}\mathbf{D} & -\mathbf{M}^{-1}\mathbf{K} \\ \mathbf{I} & \mathbf{0} \end{bmatrix} \mathbf{x}(t) + \begin{bmatrix} \mathbf{M}^{-1}\mathbf{F} \\ \mathbf{0} \end{bmatrix} \mathbf{u}(t) \\ \mathbf{y}(t) &= \begin{bmatrix} \mathbf{C} & \mathbf{G} \end{bmatrix} \mathbf{x}(t) + \mathbf{H}\mathbf{u}(t). \end{aligned} \tag{48}$$

In general, $\mathbf{J}$ is chosen to be the identity matrix. However, the following result suggests that a much better choice can be made in the context of constructing a stable ROM.

Theorem 5. If in the descriptor form (47) of the LTI system of interest $\mathbf{J}$ is chosen as $\mathbf{J} = \mathbf{K}$, then every ROM constructed by the application of a Galerkin projection to the HDM (47) is asymptotically stable.

Proof. Since the matrix $\mathbf{D}$ is SPD,

$$\begin{bmatrix} -\mathbf{D} & -\mathbf{K} \\ \mathbf{K} & \mathbf{0} \end{bmatrix} + \begin{bmatrix} -\mathbf{D} & -\mathbf{K} \\ \mathbf{K} & \mathbf{0} \end{bmatrix}^T = \begin{bmatrix} -2\mathbf{D} & \mathbf{0} \\ \mathbf{0} & \mathbf{0} \end{bmatrix} \tag{49}$$

is stable. Therefore, the direct application of Theorem 2 concludes the proof of this theorem.

Remark 3. The Lyapunov function introduced in the proof of Theorem 2 corresponds to twice the sum of the potential and kinetic energies

$$\mathcal{V}(\mathbf{x}) = \mathbf{x}^T\mathbf{E}\mathbf{x} = \begin{bmatrix} \frac{d\mathbf{z}}{dt} \\ \mathbf{z} \end{bmatrix}^T \begin{bmatrix} \mathbf{M} & \mathbf{0} \\ \mathbf{0} & \mathbf{K} \end{bmatrix} \begin{bmatrix} \frac{d\mathbf{z}}{dt} \\ \mathbf{z} \end{bmatrix} = \frac{d\mathbf{z}}{dt}^T \mathbf{M}\frac{d\mathbf{z}}{dt} + \mathbf{z}^T\mathbf{K}\mathbf{z}. \tag{50}$$

Therefore, the decay in time of this Lyapunov function is related to the decay in time of the total energy of the structural system due to damping.

Remark 4. Theorem 3 cannot be applied here because

$$\begin{bmatrix} -\mathbf{M}^{-1}\mathbf{D} & -\mathbf{M}^{-1}\mathbf{K} \\ \mathbf{I} & \mathbf{0} \end{bmatrix} + \begin{bmatrix} -\mathbf{M}^{-1}\mathbf{D} & -\mathbf{M}^{-1}\mathbf{K} \\ \mathbf{I} & \mathbf{0} \end{bmatrix}^T = \begin{bmatrix} -\mathbf{M}^{-1}\mathbf{D} - \mathbf{D}^T\mathbf{M}^{-1} & -\mathbf{M}^{-1}\mathbf{K} \\ -\mathbf{K}\mathbf{M}^{-1} & \mathbf{0} \end{bmatrix} \tag{51}$$

is not necessarily stable. For example if $\mathbf{M} = \mathbf{D} = \mathbf{K} = [1]$, the resulting matrix $\begin{bmatrix} -2 & -1 \\ -1 & 0 \end{bmatrix}$ is unstable. Hence, Theorem 2 and this remark highlight an advantage of the descriptor form of first-order LTI systems describing structural dynamics problems.

5.1.2. Analysis of a mass-damper-spring system

To illustrate the theoretical results presented above, a simple structural dynamics example is considered first. It is of the academic type, and therefore offers the advantage of being easily reproducable by the interested reader.

The structural dynamic system associated with this example problem has a one-dimensional chain structure (Figure 1(a)) with 20 blocks. Each of these, except the last one, contains four lumped masses, four dampers, and five springs. The last block contains one additional spring where an input u is applied (see Figure 1(b)). Therefore, the corresponding one-dimensional first-order LTI system, referred to here as the HDM, has $n = 160$ dof. The element properties of each block $\left(\{m_i\}_{i=1}^4,\ \{c_i\}_{i=1}^4,\ \{k_i\}_{i=1}^6\right)$, where $k_5 = 0$ except for the block where the input is applied, are given in Table 1. The input u is set to a unit step horizontal displacement applied at $t = 0$, and the response of the system is computed for $t \in [0, 100]$ s.

Two MOR methods are tested using this example: (a) a Petrov-Galerkin projection method using BPOD in the frequency domain, and (b) a Galerkin projection method using Moment Matching by Arnoldi's scheme (MMA). Each MOR method is applied to the reduction of both descriptor and non-descriptor forms of the HDM and the stability of the resulting ROMs is assessed.

BPOD is applied here using 30 complex-valued primal and 30 complex-valued dual snapshots. These are computed in the frequency domain, at evenly spaced frequencies in the interval $\omega \in [0, 2\pi]$ rad/s. Then,

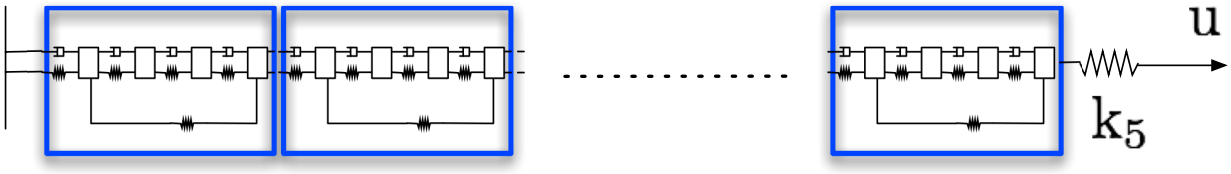

(a) Chain structure

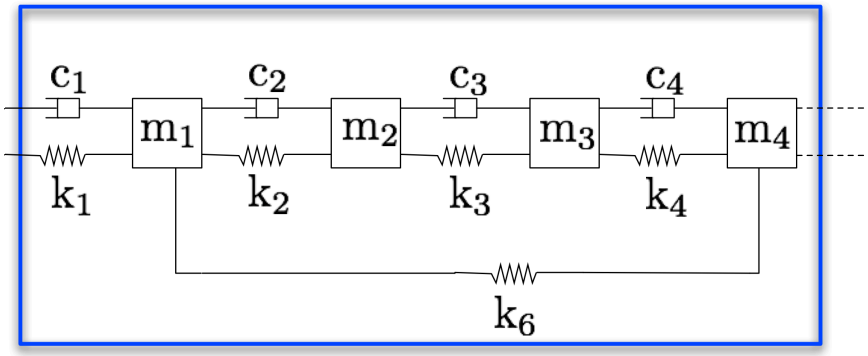

(b) Block structure

Figure 1 Mass-spring-damper system

Masses		Dampers		Springs	
	(kg)		(Ns/m)		(N/m)
m_1	125	c_1	0.1	k_1	2.2
m_2	25	c_2	1.6	k_2	1
m_3	5	c_3	0.4	k_3	3
m_4	1	c_4	0.1	k_4	9
				k_5	27
				k_6	1.2

Table 1 Mass-damper-spring system element properties.

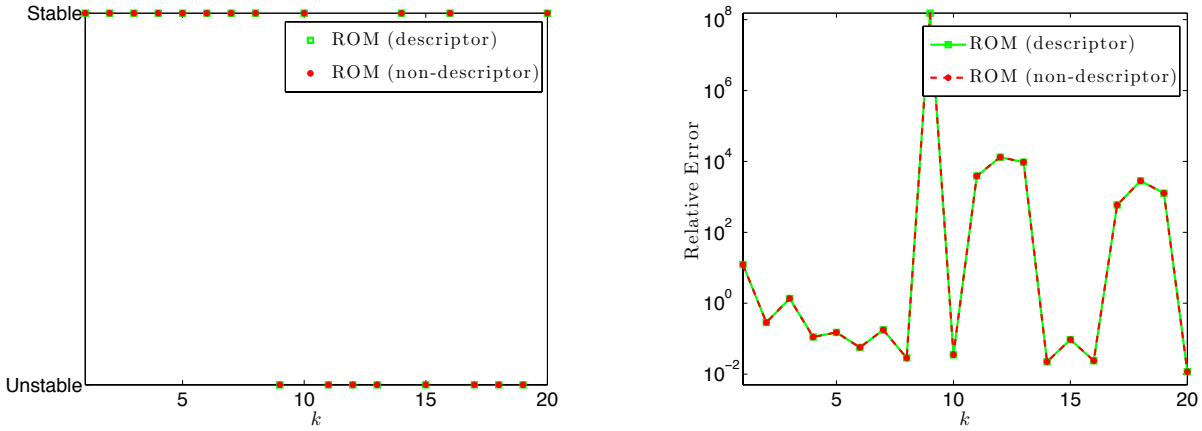

(a) Stability (b) Accuracy

Figure 2 Mass-damper-spring system: stability and accuracy of the ROMs constructed with BPOD

ROMs of dimensions $k \in \{1, \cdots, 20\}$ are constructed by Petrov-Galerkin projection. The stability of each ROM and the relative error of the solution it produces (relative to that produced by the HDM) are reported in Figure 2. The reader can observe that, as can be predicted from Theorem 4, the solutions delivered by the ROMs constructed from both descriptor and non-descriptor forms of the HDM are identical. The reader can also observe for this example that, as stated in Remark 1, the Petrov-Galerkin projection does not always preserve the stability of the HDM, even when the properties of Theorem 2 are satisfied. Figure 3(a) shows that for the reduced dimension $k = 13$, the unstable ROMs naturally lead to large relative errors. On the other hand, Figure 3(b) shows that for $k = 14$, the stable ROMs deliver highly accurate solutions.

For MMA, the moments are matched at $s_0 = 2\pi j$ and a Krylov subspace of dimension 20 is generated. Then, ROMs of dimension $k \in \{1, \cdots, 20\}$ are constructed by Galerkin projection of both descriptor and non-descriptor forms of the HDM. Figure 4 reports on the stability and accuracy exhibited by each constructed MMA ROM. As predicted by Theorem 5, all ROMs generated by the Galerkin projection of the descriptor form of the HDM are stable. The solutions they deliver are also accurate. On the other hand, most ROMs generated by the Galerkin projection of the non-descriptor form of the HDM are found to be unstable. Consequently, they deliver inaccurate solutions (see Figure 5).

5.1.3. Analysis of a butterfly MEMS system

Next, a dynamic finite element model of the butterfly MEMS gyro developed in [19] is considered here. This model has 17,361 displacement dof and the equations of interest can be written under the form (45). Therefore, the corresponding first-order LTI system has $n = 34,722$ dof. It is referred to here as the HDM of this problem. The matrices defining the governing LTI system are part of the Oberwolfach benchmark collection [20]. Step input voltages are applied to the undeformed MEMS at $t = 0$ and focus is set on the response of the dynamical system in the time-interval $t \in [0,\ 3]$ ms. More specifically, the outputs of interest are in this case the three axial displacements of the center of a detection electrode. 400 snapshots are computed in the time domain and compressed by the POD method, and a Galerkin projection is applied to reduce both descriptor and non-descriptor forms of the HDM and construct a suite of ROMs of dimension $k \in \{1, \cdots, 20\}$. The stability of these ROMs and the relative error of the solutions they produce are reported in Figure 6.

The reader can observe that, as predicted by Theorem 5, all ROMs originating from the reduction of the descriptor form of the HDM are stable. They are also very accurate. On the other hand, all ROMs originating from the non-descriptor form of the HDM are unstable and therefore inaccurate. In particular, the time-histories of the outputs predicted by both ROMs of dimension $k = 12$ and the HDM of dimension

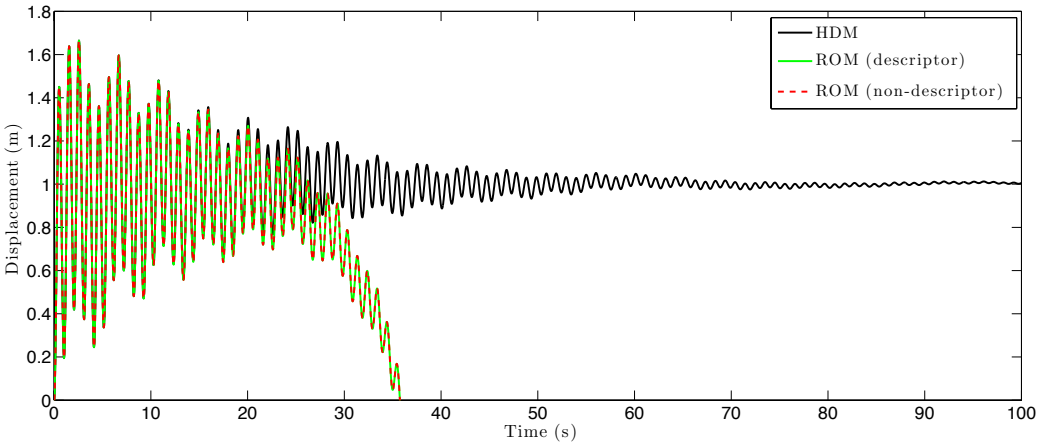

(a) $k = 13$

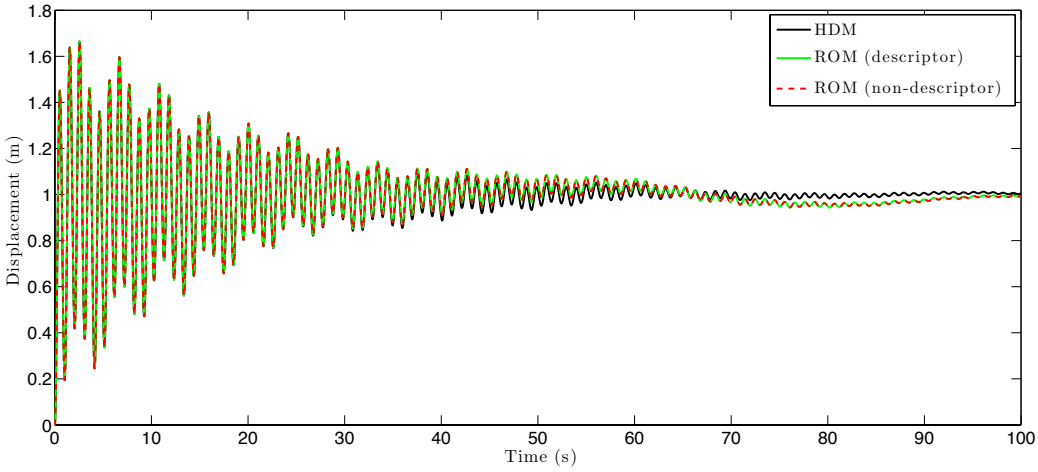

(b) $k = 14$

Figure 3 Mass-damper-spring system: time-history of the horizontal displacement of the right-most mass predicted using the ROMs constructed with BPOD

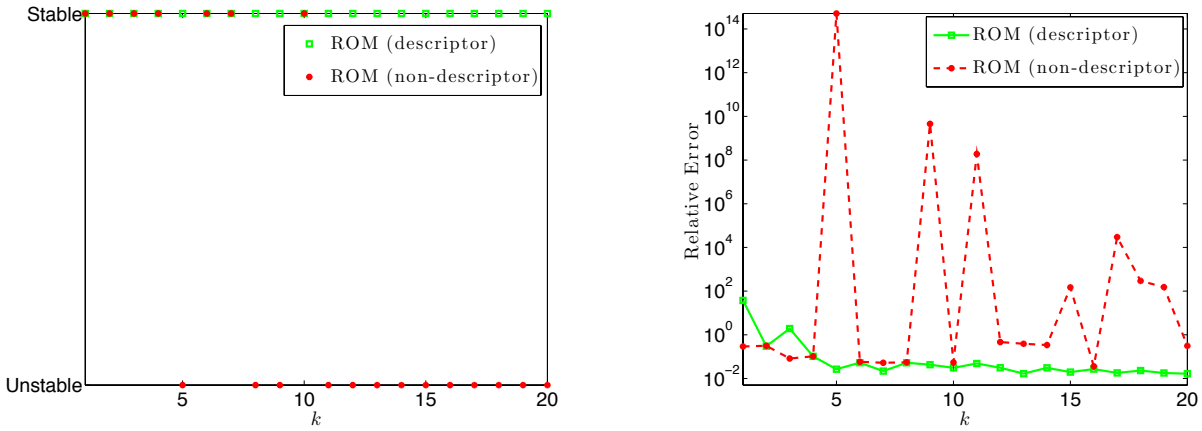

(a) Stability (b) Accuracy

Figure 4 Mass-damper-spring system: stability and accuracy of the ROMs constructed with MMA

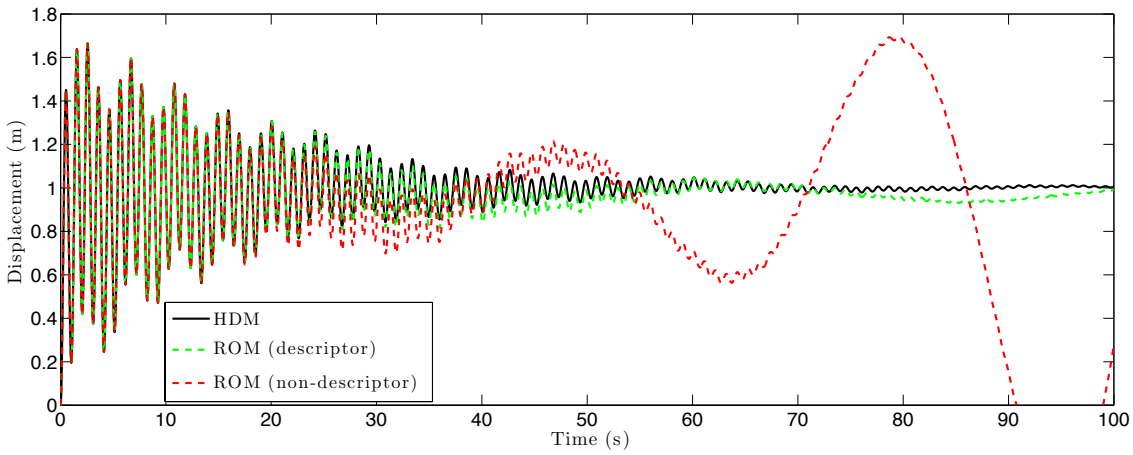

Figure 5 Mass-damper-spring system: time-history of the horizontal displacement of the right-most mass predicted using the ROMs constructed with MMA

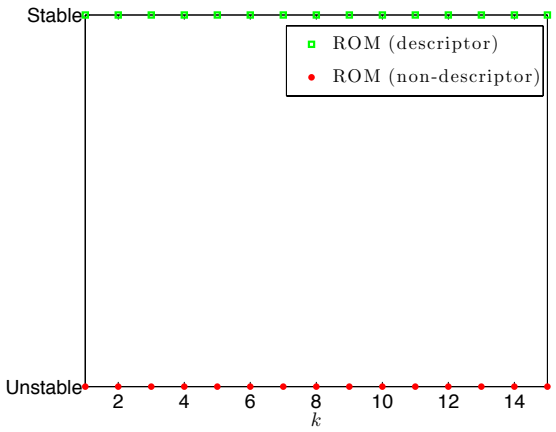

(a) Stability

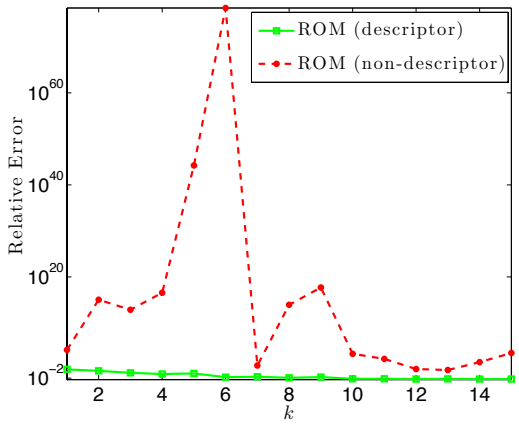

(b) Accuracy

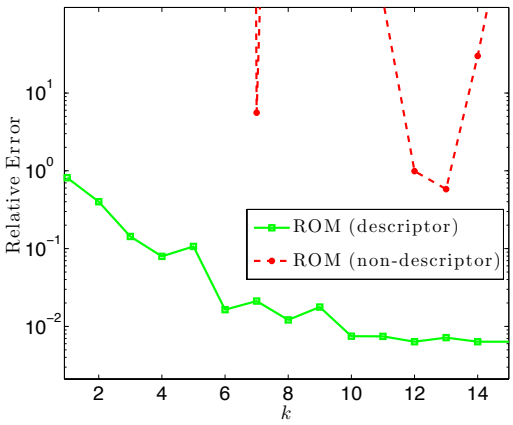

(c) Accuracy (zoom)

Figure 6 Butterfly MEMS gyro: stability and accuracy of the ROMs constructed with POD

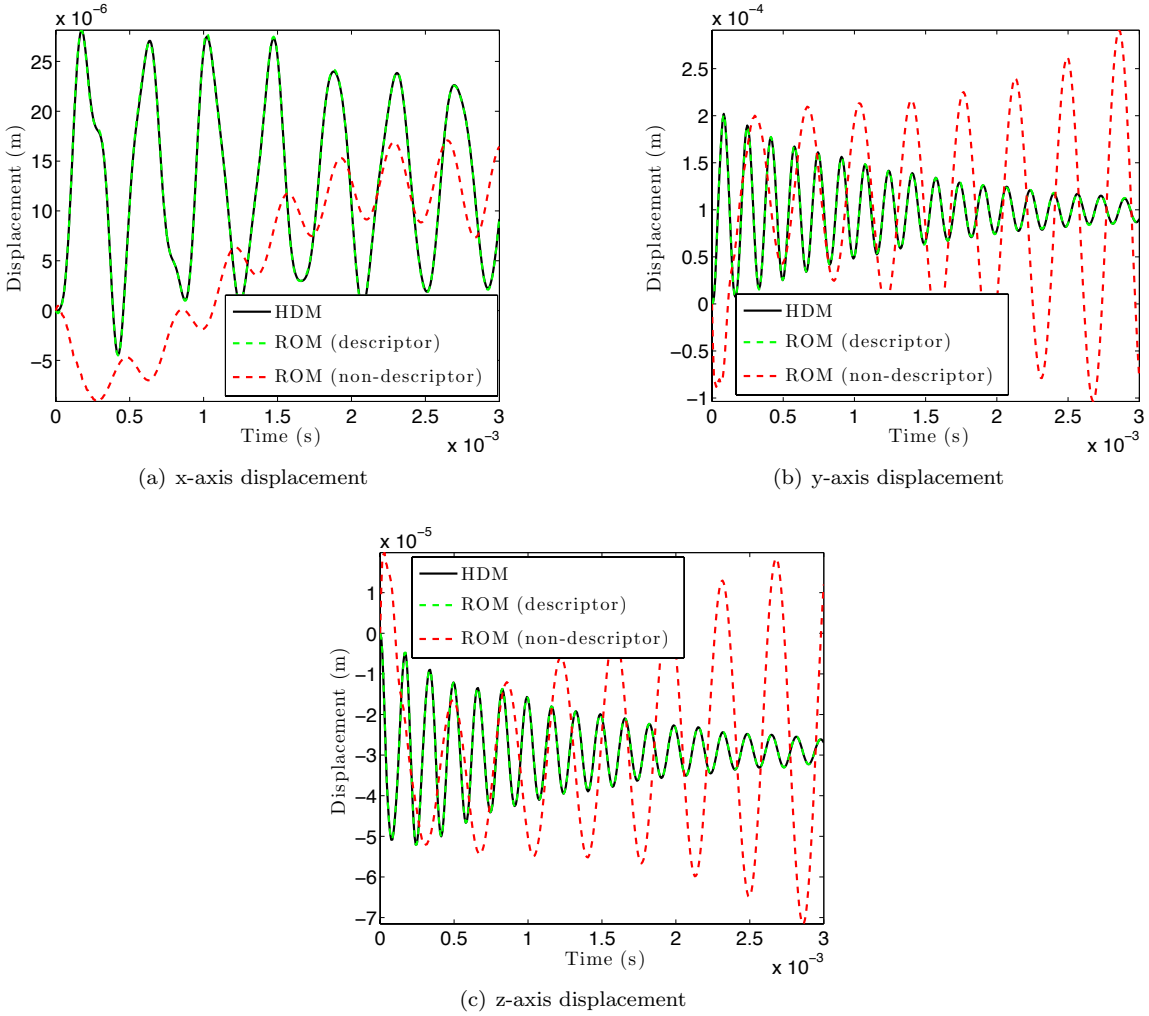

(a) x-axis displacement

(b) y-axis displacement

(c) z-axis displacement

Figure 7 Butterfly MEMS gyro: time-histories of the x, y, and z displacements of the center of a detection electrode predicted using the ROMs of dimension $k = 12$ constructed with POD

$n = 34,722$ are reported in Figure 7. Whereas the predictions delivered by the ROM originating from the descriptor form of the HDM reproduces with great accuracy their counterparts delivered by the HDM, those obtained using the ROM originating from the non-descriptor form are inaccurate and unstable.

5.2. Dynamic fluid-structure interaction

5.2.1. LTI subsystems and coupled LTI system of interest

Linearized CFD-based computational methods for the solution of coupled fluid-structure interaction problems are rapidly becoming the preferred methods for the flutter analysis of modern aircraft in transonic and other nonlinear regimes. Here, the linearized, CFD-based computational framework for fluid-structure interaction developed first in [21] is adopted for this purpose. In this framework, a structural subsystem is modeled as an LTI subsystem of the form (45); its dimension is denoted by n_s. For aeroelastic analysis, a reduced version of this LTI subsystem is typically constructed using a ROB constituted of the first k_s natural

mode shapes of the structure and a Galerkin projection. Hence, such a reduced system can be written as

$$\mathbf{I}_{k_s}\frac{d^2\mathbf{z}_{k_s}}{dt^2}(t)+\mathbf{D}_{k_s}\frac{d\mathbf{z}_{k_s}}{dt}(t)+\mathbf{\Omega}_{k_s}^2\mathbf{z}_{k_s}(t)=\sqrt{p_\infty}\mathbf{F}_{k_s}\mathbf{x}(t), \tag{52}$$

where $\mathbf{z}_{k_s}\in\mathbb{R}^{k_s}$ is the vector of generalized (modal) coordinates, $\mathbf{\Omega}_{k_s}$ is the diagonal matrix of natural circular frequencies of the structure, $\mathbf{D}_{k_s}\in\mathbb{R}^{k_s\times k_s}$ is the generalized damping matrix, p_∞ is the free-stream pressure, n_f the dimension of the fluid LTI subsystem described below, $\mathbf{x}\in\mathbb{R}^{n_f}$ its state, and $\mathbf{F}_{k_s}\in\mathbb{R}^{k_s\times n_f}$ the generalized Jacobian of the aerodynamic forces acting on the structure with respect to the fluid state vector $\mathbf{x}$.

For simplicity, the flow is assumed here to be inviscid. Hence, it is modeled by the linearization of the Euler equations around a steady-state equilibrium characterized by the free-stream pressure p_∞ and density ρ_∞, among others. This modelization leads to a fluid LTI subsystem which can be written as

$$\mathbf{E}\frac{d\mathbf{x}}{dt}(t)=\sqrt{\frac{p_\infty}{\rho_\infty}}\mathbf{A}\mathbf{x}(t)+\sqrt{\frac{p_\infty}{\rho_\infty}}\mathbf{G}_{k_s}\mathbf{z}_{k_s}(t)+\mathbf{C}_{k_s}\frac{d\mathbf{z}_{k_s}}{dt}(t), \tag{53}$$

where $\mathbf{E}\in\mathbb{R}^{n_f\times n_f}$ is the diagonal matrix of control volumes of the CFD mesh, $\mathbf{A}\in\mathbb{R}^{n_f\times n_f}$ is the Jacobian of the fluxes with respect to the fluid state evaluated at the steady-state equilibrium solution, and $\mathbf{G}_{k_s}\in\mathbb{R}^{n_f\times k_s}$ and $\mathbf{C}_{k_s}\in\mathbb{R}^{n_f\times k_s}$ are two fluid-structure coupling matrices modeling the interaction of the fluid subsystem with the dynamics of the structure.

Fluid snapshots are generated in the frequency domain by exciting, for a given set of frequencies, the wall boundary of the fluid subsystem by one or several structural modal displacement fields. These snapshots are compressed using the POD method to construct a ROB $\mathbf{V}_{k_f}\in\mathbb{R}^{n_f\times k_f}$, and the fluid state is approximated using this ROB as

$$\mathbf{x}(t)\approx\mathbf{V}_{k_f}\mathbf{x}_{k_f}(t), \tag{54}$$

where $\mathbf{x}_{k_f}\in\mathbb{R}^{k_f}$.

When the fluid LTI subsystem is expressed in descriptor form as in (53), its Galerkin projection onto $\mathbf{V}_{k_f}$ leads to the following ROM of dimension k_f

$$\frac{d\mathbf{x}_{k_f}}{dt}(t)=\sqrt{\frac{p_\infty}{\rho_\infty}}\left(\mathbf{V}_{k_f}^T\mathbf{A}\mathbf{V}_{k_f}\right)\mathbf{x}_{k_f}(t)+\sqrt{\frac{p_\infty}{\rho_\infty}}\mathbf{V}_{k_f}^T\mathbf{G}_{k_s}\mathbf{z}_{k_s}(t)+\mathbf{V}_{k_f}^T\mathbf{C}_{k_s}\frac{d\mathbf{z}_{k_s}}{dt}(t). \tag{55}$$

When Eq. (53) is recast in non-descriptor form and subsequently projected onto the trial ROB $\mathbf{V}_{k_f}$, the following alternative ROM is obtained

$$\frac{d\mathbf{x}_{k_f}}{dt}(t)=\sqrt{\frac{p_\infty}{\rho_\infty}}\left(\mathbf{V}_{k_f}^T\mathbf{E}^{-1}\mathbf{A}\mathbf{V}_{k_f}\right)\mathbf{x}_{k_f}(t)+\sqrt{\frac{p_\infty}{\rho_\infty}}\left(\mathbf{V}_{k_f}^T\mathbf{E}^{-1}\mathbf{G}_{k_s}\right)\mathbf{z}_{k_s}(t)+\left(\mathbf{V}_{k_f}^T\mathbf{E}^{-1}\mathbf{C}_{k_s}\right)\frac{d\mathbf{z}_{k_s}}{dt}(t). \tag{56}$$

In both cases, the reduced fluid subsystem can be written in the generic form

$$\frac{d\mathbf{x}_{k_f}}{dt}(t)=\sqrt{\frac{p_\infty}{\rho_\infty}}\mathbf{A}_{k_f}\mathbf{x}_{k_f}(t)+\sqrt{\frac{p_\infty}{\rho_\infty}}\mathbf{G}_{k_f,k_s}\mathbf{z}_{k_s}(t)+\mathbf{C}_{k_f,k_s}\frac{d\mathbf{z}_{k_s}}{dt}(t), \tag{57}$$

where $\mathbf{A}_{k_f}\in\mathbb{R}^{k_f\times k_f}$, $\mathbf{G}_{k_f,k_s}\in\mathbb{R}^{k_f\times k_s}$ and $\mathbf{C}_{k_f,k_s}\in\mathbb{R}^{k_f\times k_s}$.

Substituting Eq. (54) into the reduced structural subsystem (52) leads to the following structural ROM

$$\mathbf{I}_{k_s}\frac{d^2\mathbf{z}_{k_s}}{dt^2}(t)+\mathbf{D}_{k_s}\frac{d\mathbf{z}_{k_s}}{dt}(t)+\mathbf{\Omega}_{k_s}^2\mathbf{z}_{k_s}(t)=\sqrt{p_\infty}\mathbf{F}_{k_s,k_f}\mathbf{x}_{k_f}(t), \tag{58}$$

where $\mathbf{F}_{k_s,k_f}=\mathbf{F}_{k_s}\mathbf{V}_{k_f}\in\mathbb{R}^{k_s\times k_f}$.

Re-writing Eq. (58) in first-order form and combining the result and Eq. (57) into a single LTI system leads to the following coupled fluid-structure linear(ized) ROM of size k_f+2k_s

$$\frac{d}{dt}\begin{bmatrix}\mathbf{x}_{k_f}\\ \frac{d\mathbf{z}_{k_s}}{dt}\\ \mathbf{z}_{k_s}\end{bmatrix}=\begin{bmatrix}\sqrt{\frac{p_\infty}{\rho_\infty}}\mathbf{A}_{k_f} & \begin{bmatrix}\mathbf{C}_{k_f,k_s} & \sqrt{\frac{p_\infty}{\rho_\infty}}\mathbf{G}_{k_f,k_s}\end{bmatrix}\\ \begin{bmatrix}\sqrt{p_\infty}\mathbf{F}_{k_s,k_f}\\ \mathbf{0}\end{bmatrix} & \begin{bmatrix}-\mathbf{D}_{k_s} & -\mathbf{\Omega}_{k_s}^2\\ \mathbf{I}_{k_s} & \mathbf{0}\end{bmatrix}\end{bmatrix}\begin{bmatrix}\mathbf{x}_{k_f}\\ \frac{d\mathbf{z}_{k_s}}{dt}\\ \mathbf{z}_{k_s}\end{bmatrix}. \tag{59}$$

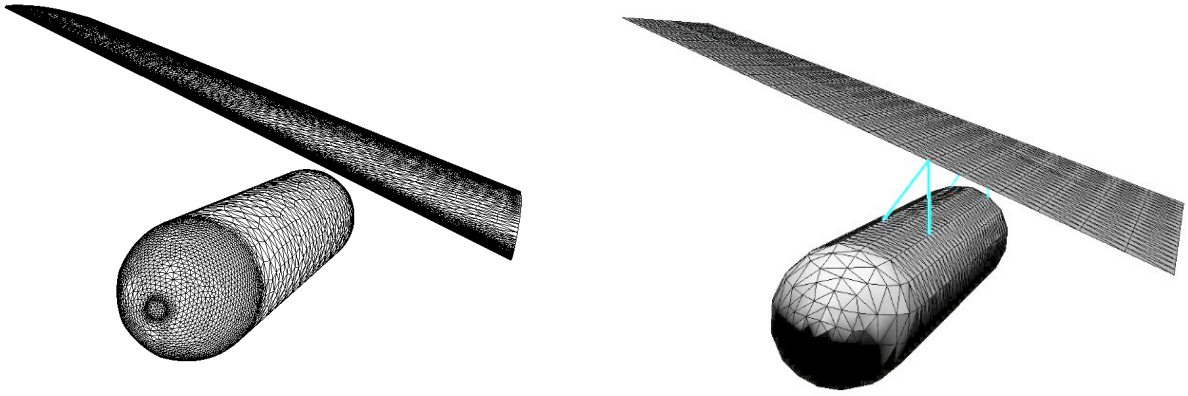

(a) CFD surface grid (b) Finite element structural model

Figure 8 High-dimensional aeroelastic model of a wing-store configuration

Using the above ROM, the onset of flutter can be established by fixing the free-stream density ρ_∞ and increasing the free-stream pressure p_∞ until this ROM becomes unstable. At that point, the free-stream pressure reaches a value known as a critical free-stream pressure p_∞^{cr}. This fast approach to flutter analysis requires however that the coupled fluid-structure ROM (59) be stable outside the flutter point. In [10], it was shown that this in turn requires that the reduced fluid matrix $\mathbf{A}_{k_f}$ be stable. Hence, this application highlights the importance of requiring that a projection-based MOR method preserves the stability of the LTI system or subsystem to which it is applied.

5.2.2. Flutter analysis of a wing-store-fuel configuration

Consider first the aeroelastic wing-store-fuel configuration described in [22] and graphically depicted in Figure 8. For a fixed altitude, a flight condition for this configuration is defined here by a pair of free-stream Mach number M_∞ and fuel fill level in the store (or tank). The hydroelastic effects due to the presence of fuel inside the tank modify the structural properties of the system and affect its aeroelastic characteristics. The fluid and structural HDMs developed in [22] for this aeroelastic configuration have the dimensions $n_f = 689,485$ and $n_s = 6,834$, respectively.

For every flight condition of interest, 44 real-valued fluid snapshots are generated by exciting the wall boundary of the structural subsystem by each of its first $k_s = 4$ structural mode shapes at each of six equispaced reduced frequencies in the interval $[0, 0.0125]$. Then, these snapshots are compressed by the POD method to construct a suite of fluid ROBs of dimension $k_f \in \{1, \cdots, 40\}$, and a corresponding suite of fluid ROMs of same dimension k_f is constructed by the Galerkin projection of both descriptor and non-descriptor forms of the fluid LTI subsystem onto these ROBs.

In all cases, the structural ROM is constructed as in (58) with $k_s = 4$ and re-written in first-order form.

The first considered flight condition is defined by $M_\infty = 0.95$ and an empty tank. In this case, Figure 9(a) reports on the stability of the constructed fluid ROMs, and Figure 9(b) on the accuracy they deliver for the prediction of the critical pressure. Again, all fluid ROMs originating from the descriptor form of the fluid LTI subsystem are found to be stable. On the other hand, the fluid ROMs of dimension $k_f \in \{29, 36, 37, 38\}$ originating from the non-descriptor form of the fluid LTI subsystem are found to be unstable. Consequently, each unstable fluid ROM leads to an erroneous prediction of the critical pressure using the coupled fluid-structure (or aeroelastic) ROM (59) (see Figure 9(b)). In contrast, all aeroelastic ROMs of dimension $k_f \geq 15$ originating from the descriptor form of the fluid LTI subsystem deliver accurate predictions of the critical pressure. Similar results were also reported in [23] where a preliminary study of this problem was

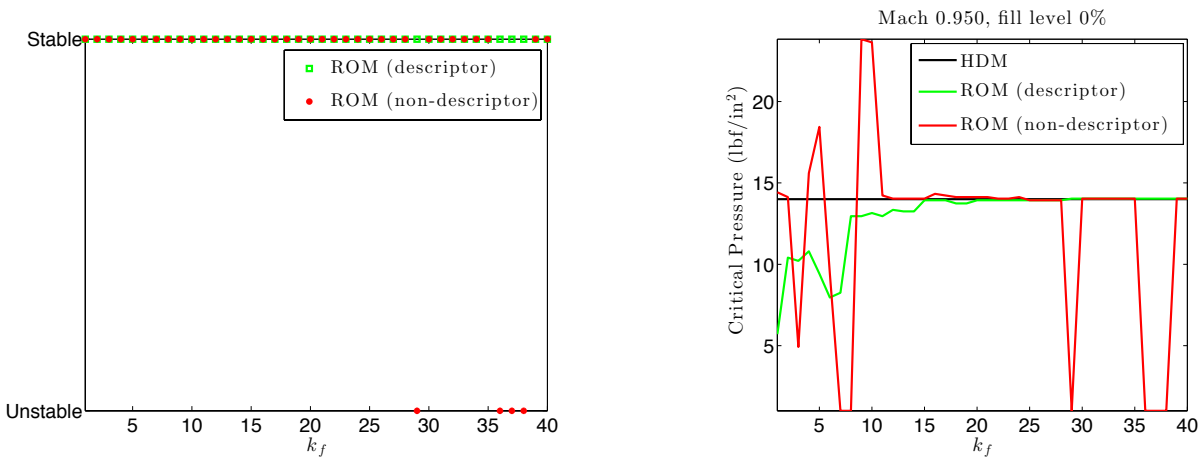

(a) Stability

(b) Accuracy

Figure 9 Wing-store configuration ($M_\infty = 0.95$ and empty tank): stability of the fluid ROM as a function of its size, and accuracy of the critical free-stream pressure predicted using the corresponding aeroelastic ROM

first performed.

The second and third considered flight conditions are defined by $M_\infty = 1.1$ and 31% fuel fill level in the tank, and $M_\infty = 0.75$ and 69% fuel fill level, respectively. Figures 10 and 11 report on the stability of the constructed fluid ROMs and accuracy of the corresponding aeroelastic ROMs for these two cases, respectively. These figures confirm the trends observed for the first flight condition and lead to similar conclusions.

5.2.3. Aeroelastic analysis of an F/A-18 aircraft configuration

Next, an aeroelastic HDM of a full F/A-18 configuration with tip missiles is considered (see Figure 12). Here, the dimension of the fluid HDM is $n_f = 3,583,095$, and that of the structural HDM is $n_s = 11,290$. The latter is reduced by the Galerkin projection on a modal basis with $k_s = 10$ structural mode shapes.

410 real-valued fluid snapshots are computed in the frequency domain by exciting the wall boundary of the aircraft configuration with all k_s structural modal displacements at 21 equispaced reduced frequencies in the interval $[0, 0.04]$. These snapshots are compressed by the POD method to construct a suite of ROBs and two corresponding suites of fluid ROMs of dimension $k_f \in \{1, \cdots, 400\}$: one by Galerkin projection of the descriptor form of the coupled fluid-structure LTI system, and one by Galerkin projection of its non-descriptor form. The stability of the constructed fluid ROMs is assessed and the obtained results are reported in Figure 13. Once again, all fluid ROMs originating from the descriptor form of the fluid LTI subsystem are stable, but more than half those originating from its non-descriptor form are unstable.

6. Conclusions

The majority of model order reduction methods do not preserve the stability properties of the large-scale linear time-invariant dynamical systems to which they are applied. Stabilization procedures have been recently proposed [11, 10] to address this issue. However, these procedures have limitations and do not necessarily lead to best-practices in model order reduction. This paper contributes to this topic theoretical and numerical experiment results that show that the reduction of the descriptor form of large-scale linear time-invariant dynamical systems by Galerkin projection preserves their stability under mild assumptions that are satisfied, for example, by structural dynamic systems. This suggests that instability in model order reduction by Galerkin projection is often caused by the popular reduction of the non-descriptor form of the dynamical system of interest, instead of its descriptor form. This suggestion is furthermore supported

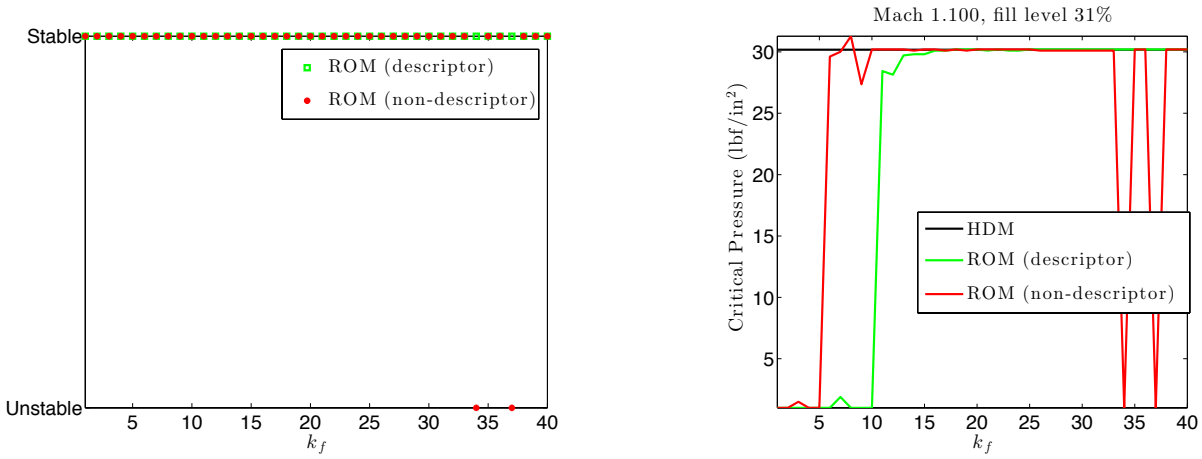

(a) Stability (b) Accuracy

Figure 10 Wing-store configuration ($M_\infty = 1.1$ and 31% fuel fill level): stability of the fluid ROM as a function of its size, and accuracy of the critical free-stream pressure predicted using the corresponding aeroelastic ROM

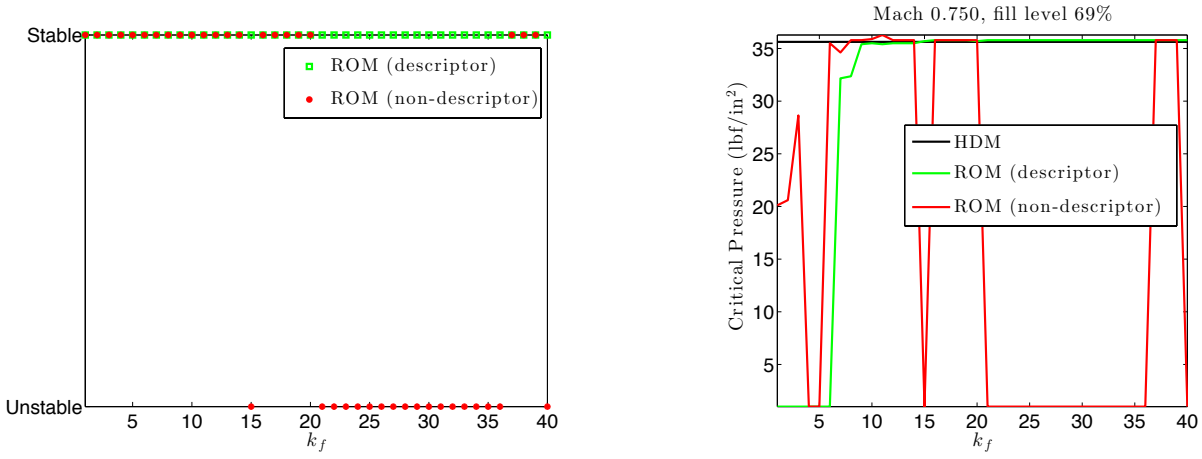

(a) Stability (b) Accuracy

Figure 11 Wing-store configuration ($M_\infty = 0.75$ and 69% fuel fill level): stability of the fluid ROM as a function of its size, and accuracy of the critical free-stream pressure predicted using the corresponding aeroelastic ROM

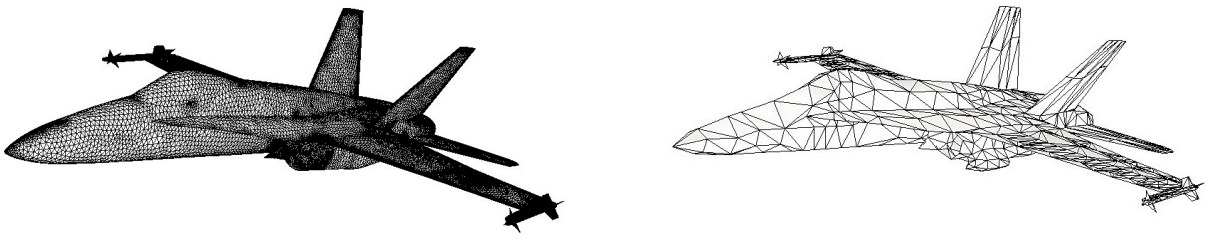

(a) CFD surface grid (b) FE structural model

Figure 12 Aeroelastic HDM of a full F18/A configuration

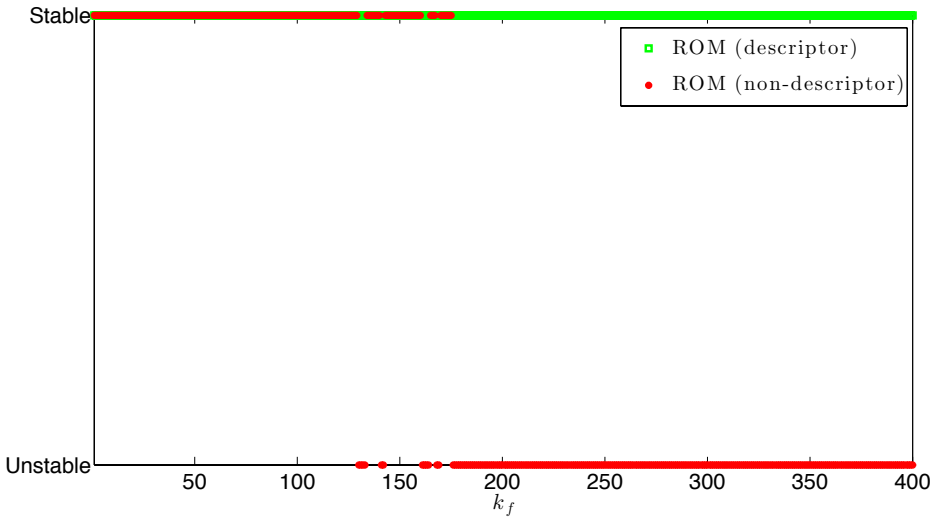

Figure 13 F18/A configuration at $M_\infty = 0.99$: stability of the fluid ROM as a function of its size

in this paper by numerous results from different applications obtained using various popular model order reduction techniques such as Proper Orthogonal Decomposition, Balanced Proper Orthogonal Decomposition, and Moment Matching. Other theoretical and experimental results presented in this paper also lead to recommending performing model order reduction on the descriptor rather than non-descriptor form of the governing equations, using preferrably a Galerkin projection except when problem specific requirements such as those discussed in [24] prevents it.

7. Appendix: Proof of Theorem 4

First, the following lemma is stated and proved.

Lemma 1. In the descriptor case, the dual snapshots satisfy

$$\mathrm{Re}\left(\mathbf{z}(-\omega)\right) = \mathrm{Re}\left(\mathbf{z}(\omega)\right),\ \mathrm{Im}\left(\mathbf{z}(-\omega)\right) = -\mathrm{Im}\left(\mathbf{z}(\omega)\right) \tag{60}$$

and as a result, the dual snapshot matrix satisfies

$$\mathbf{Z}^d(-\omega_1, \cdots, -\omega_{N_{\text{snaps}}}) = \mathbf{Z}^d(\omega_1, \cdots, \omega_{N_{\text{snaps}}}) \begin{bmatrix} \mathbf{I}_{N_{\text{snaps}}} & \mathbf{0} \\ \mathbf{0} & -\mathbf{I}_{N_{\text{snaps}}} \end{bmatrix}. \tag{61}$$

Proof of Lemma 1. For $\omega = 0$, the result is straightforward. Let $\omega \neq 0$. Then, $\mathrm{Re}\left(\mathbf{z}^d(\omega)\right)$ and $\mathrm{Im}\left(\mathbf{z}^d(\omega)\right)$ are solutions of

$$\begin{aligned} \left(\omega^2\mathbf{E}^T + \mathbf{A}^T\mathbf{E}^{-T}\mathbf{A}^T\right)\mathrm{Im}\left(\mathbf{z}^d(\omega)\right) &= -\omega\mathbf{C}^T \\ \mathrm{Re}\left(\mathbf{z}^d(\omega)\right) &= \frac{1}{\omega}\mathbf{E}^{-T}\mathbf{A}^T\mathrm{Im}\left(\mathbf{z}^d(\omega)\right). \end{aligned} \tag{62}$$

Similarly, $\mathrm{Re}\left(\mathbf{z}^d(-\omega)\right)$ and $\mathrm{Im}\left(\mathbf{z}^d(-\omega)\right)$ are solutions of

$$\begin{aligned} \left(\omega^2\mathbf{E}^T + \mathbf{A}^T\mathbf{E}^{-T}\mathbf{A}^T\right)\mathrm{Im}\left(\mathbf{z}^d(-\omega)\right) &= \omega\mathbf{C}^T \\ \mathrm{Re}\left(\mathbf{z}^d(-\omega)\right) &= -\frac{1}{\omega}\mathbf{E}^{-T}\mathbf{A}^T\mathrm{Im}\left(\mathbf{z}^d(-\omega)\right), \end{aligned} \tag{63}$$

which concludes the proof of this lemma.

Proof of Theorem 4. From the previous lemma and Eq. (38), it follows that

$$\mathbf{Z}^{nd}(\omega_1, \cdots, \omega_{N_{\text{snaps}}}) = \mathbf{E}^T\mathbf{Z}^d(-\omega_1, \cdots, -\omega_{N_{\text{snaps}}}) = \mathbf{E}^T\mathbf{Z}^d(\omega_1, \cdots, \omega_{N_{\text{snaps}}}) \begin{bmatrix} \mathbf{I}_{N_{\text{snaps}}} & \mathbf{0} \\ \mathbf{0} & -\mathbf{I}_{N_{\text{snaps}}} \end{bmatrix}. \tag{64}$$

Hence, the product of the dual and primal snapshot matrices is, in the non-descriptor case,

$$\mathbf{Z}^{nd^T}\mathbf{X} = \begin{bmatrix} \mathbf{I}_{N_{\text{snaps}}} & \mathbf{0} \\ \mathbf{0} & -\mathbf{I}_{N_{\text{snaps}}} \end{bmatrix} \mathbf{Z}^{d^T}\mathbf{E}\mathbf{X} = \begin{bmatrix} \mathbf{I}_{N_{\text{snaps}}} & \mathbf{0} \\ \mathbf{0} & -\mathbf{I}_{N_{\text{snaps}}} \end{bmatrix} \mathbf{\Psi}^d\mathbf{\Sigma}^d\mathbf{\Phi}^d. \tag{65}$$

The last equality is an SVD of the product $\mathbf{Z}^{nd^T}\mathbf{X}$. Eq. (40) provides another SVD of the same matrix. The SVD is not unique; however, assuming that the k-th and $k+1$-th singular values are distinct, the following relationship exists between the components of the two SVDs [25]

$$\mathbf{\Psi}_k^{nd} = \begin{bmatrix} \mathbf{I}_{N_{\text{snaps}}} & \mathbf{0} \\ \mathbf{0} & -\mathbf{I}_{N_{\text{snaps}}} \end{bmatrix} \mathbf{\Psi}_k^d\mathbf{Q},\ \mathbf{\Sigma}_k^{nd} = \mathbf{\Sigma}_k^d,\ \mathbf{\Phi}_k^{nd} = \mathbf{\Phi}_k^d\mathbf{Q}, \tag{66}$$

where $\mathbf{Q} \in \mathbb{R}^{k\times k}$ is a block diagonal orthogonal matrix that satisfies $\mathbf{Q}\mathbf{\Sigma}_k^d\mathbf{Q}^T = \mathbf{\Sigma}_k^d$. As a result, $\mathbf{Q}$ and $\mathbf{\Sigma}^d$ satisfy $\mathbf{Q}\mathbf{\Sigma}_k^{d^{-\frac{1}{2}}}\mathbf{Q}^T = \mathbf{\Sigma}_k^{d^{-\frac{1}{2}}}$ as well.

Therefore, the trial ROBs for both descriptor and non-descriptor forms are related by

$$\mathbf{V}_k^{nd} = \mathbf{X}\mathbf{\Phi}_k^{nd}\mathbf{\Sigma}_k^{nd^{-\frac{1}{2}}} = \mathbf{X}\mathbf{\Phi}_k^{d}\mathbf{Q}\mathbf{\Sigma}_k^{d^{-\frac{1}{2}}} = \mathbf{X}\mathbf{\Phi}_k^{d}\mathbf{\Sigma}_k^{d^{-\frac{1}{2}}}\mathbf{Q} = \mathbf{V}_k^{d}\mathbf{Q}. \tag{67}$$

Similarly, the test ROBs satisfy

$$\mathbf{W}_k^{nd} = \mathbf{Z}^{nd}\mathbf{\Psi}_k^{nd}\mathbf{\Sigma}_k^{nd^{-\frac{1}{2}}} = \mathbf{E}^T\mathbf{Z}^{d}\begin{bmatrix}\mathbf{I}_{N_{\text{snaps}}} & \mathbf{0}\\ \mathbf{0} & -\mathbf{I}_{N_{\text{snaps}}}\end{bmatrix}\begin{bmatrix}\mathbf{I}_{N_{\text{snaps}}} & \mathbf{0}\\ \mathbf{0} & -\mathbf{I}_{N_{\text{snaps}}}\end{bmatrix}\mathbf{\Psi}_k^{d}\mathbf{Q}\mathbf{\Sigma}_k^{d^{-\frac{1}{2}}} = \mathbf{E}^T\mathbf{Z}^{d}\mathbf{\Psi}_k^{d}\mathbf{\Sigma}_k^{d^{-\frac{1}{2}}}\mathbf{Q} = \mathbf{E}^T\mathbf{W}_k^{d}\mathbf{Q}. \tag{68}$$

Hence, the equivalent HDM (20) reconstructed from the reduction of the non-descriptor form of the governing LTI system using BPOD can also be written as

$$\begin{aligned}\frac{d\widehat{\mathbf{x}}}{dt}(t) &= \left(\mathbf{V}_k^{d}\mathbf{Q}\mathbf{Q}^T\mathbf{W}_k^{d^T}\mathbf{E}\mathbf{E}^{-1}\mathbf{A}\right)\widehat{\mathbf{x}}(t) + \left(\mathbf{V}_k^{d}\mathbf{Q}^T\mathbf{Q}\mathbf{W}_k^{d^T}\mathbf{E}\mathbf{E}^{-1}\mathbf{B}\right)\mathbf{u}(t)\\ \mathbf{y}(t) &= \mathbf{C}\widehat{\mathbf{x}}(t) + \mathbf{D}\mathbf{u}(t),\end{aligned} \tag{69}$$

or

$$\begin{aligned}\frac{d\widehat{\mathbf{x}}}{dt}(t) &= \left(\mathbf{V}_k^{d}\mathbf{W}_k^{d^T}\mathbf{A}\right)\widehat{\mathbf{x}}(t) + \left(\mathbf{V}_k^{d}\mathbf{W}_k^{d^T}\mathbf{B}\right)\mathbf{u}(t)\\ \mathbf{y}(t) &= \mathbf{C}\widehat{\mathbf{x}}(t) + \mathbf{D}\mathbf{u}(t).\end{aligned} \tag{70}$$

The above system is the equivalent HDM (14) reconstructed from the reduction of the descriptor form of the governing LTI system using BPOD, which concludes the proof of Theorem 4.

Acknowledgments

The authors acknowledge partial support by the Army Research Laboratory through the Army High Performance Computing Research Center under Cooperative Agreement W911NF-07-2-0027, partial support by the Office of Naval Research under Grant N00014-11-1-0707, partial support by a research grant from King Abdulaziz City for Science and Technology (KACST), and partial support by The Boeing Company under Contract Sponsor Ref. 45047. The content of this publication does not necessarily reflect the position or policy of any of these supporters, and no official endorsement should be inferred.

References

[1] B. Moore, Principal component analysis in linear systems: Controllability, observability, and model reduction, IEEE Transactions on Automatic Control 26 (1981).

[2] E. J. Grimme, Krylov projection methods for model reduction, Ph.D. Thesis, University of Illinois at Urbana Champaign, 1997.

[3] T. Kim, Frequency-domain Karhunen-Loeve method and its application to linear dynamic systems, AIAA JOURNAL 36 (1998) 2117–2123.

[4] K. Willcox, J. Peraire, Balanced model reduction via the proper orthogonal decomposition, AIAA JOURNAL 40 (2002) 2323–2330.

[5] T. Lieu, C. Farhat, M. Lesoinne, Reduced-order fluid/structure modeling of a complete aircraft configuration, Computer Methods in Applied Mechanics and Engineering 195 (2009) 5730–5742.

[6] T. Lieu, C. Farhat, Adaptation of aeroelastic reduced-order models and application to an F-16 configuration, AIAA JOURNAL 45 (2007) 1244–1257.

[7] D. Amsallem, C. Farhat, Interpolation method for adapting reduced-order models and application to aeroelasticity, AIAA JOURNAL 46 (2008) 1803–1813.

[8] D. Amsallem, J. Cortial, C. Farhat, Toward real-time computational-fluid-dynamics-based aeroelastic computations using a database of reduced-order information, AIAA JOURNAL 48 (2010) 2029–2037.

[9] T. Bui-Thanh, K. Willcox, O. Ghattas, B. van Bloemen Waanders, Goal-oriented, model-constrained optimization for reduction of large-scale systems, Journal of Computational Physics 224 (2007) 880–896.

[10] D. Amsallem, C. Farhat, Stabilization of projection-based reduced-order models, International Journal for Numerical Methods in Engineering 91 (2012) 358–377.

[11] B. N. Bond, L. Daniel, Guaranteed stable projection-based model reduction for indefinite and unstable linear systems, in: 2008 IEEE/ACM International Conference on Computer-Aided Design (ICCAD), IEEE, 2008, pp. 728–735.

[12] T. Stykel, Analysis and numerical solution of generalized Lyapunov equations, Institut für Mathematik, Technische Universität, Berlin (2002).

[13] M. Heinkenschloss, D. C. Sorensen, K. Sun, Balanced truncation model reduction for a class of descriptor systems with application to the Oseen equations, SIAM Journal on Scientific Computing 30 (2008) 1038.

[14] A. Antoulas, Approximation of large-scale dynamical systems, SIAM (2005).

[15] L. Sirovich, Turbulence and the dynamics of coherent structures. Part I: Coherent structures, Quarterly of applied mathematics 45 (1987) 561–571.

[16] C. W. Rowley, Model reduction for fluids, using balanced proper orthogonal decomposition, International Journal on Bifurcation and Chaos 15 (2005) 997–1013.

[17] U. Hetmaniuk, R. Tezaur, C. Farhat, Review and assessment of interpolatory model order reduction methods for frequency response structural dynamics and acoustics problems, International Journal for Numerical Methods in Engineering 90 (2012) 1636–1662.

[18] U. Hetmaniuk, R. Tezaur, C. Farhat, An adaptive scheme for a class of interpolatory model reduction methods for frequency response problems, International Journal for Numerical Methods in Engineering to appear (2012).

[19] J. Lienemann, D. Billger, E. B. Rudnyi, A. Greiner, J. G. Korvink, MEMS compact modeling meets model order reduction: Examples of the application of Arnoldi methods to microsystem devices, Technical Proceedings of the 2004 Nanotechnology Conference and Trade Show (2004).

[20] Oberwolfach benchmark collection, http://portal.uni-freiburg.de/imteksimulation/downloads/benchmark/ (2005).

[21] M. Lesoinne, M. Sarkis, U. Hetmaniuk, C. Farhat, A linearized method for the frequency analysis of three-dimensional fluid/structure interaction problems in all flow regimes, Computer Methods in Applied Mechanics and Engineering 190 (2001) 3121–3146.

[22] E. Chiu, C. Farhat, Effects of fuel slosh on flutter prediction, AIAA 2009-2682, 50th AIAA/ASME/ASCE/AHS/ASC Structures, Structural Dynamics, and Materials Conference (2009).

[23] D. Amsallem, C. Farhat, On the stability of linearized reduced-order models: descriptor vs. non-descriptor form and application to fluid-structure interaction, AIAA Paper 2012-2687, 42nd AIAA Fluid Dynamics Conference and Exhibit. 25-28 June 2012, New Orleans, Louisiana (2012) 1–12.

[24] K. Carlberg, C. Bou-Mosleh, C. Farhat, Efficient non-linear model reduction via a least-squares Petrov–Galerkin projection and compressive tensor approximations, International Journal for Numerical Methods in Engineering 86 (2011) 155–181.

[25] R. A. Horn, C. R. Johnson, Topics in Matrix Analysis, Cambridge Univ Press, 1994.